NUMERICAL MODELLING OF THE PROPAGATION ENVIRONMENT IN THE ATMOSPHERIC BOUNDARY LAYER OF LITTORAL AREAS

Resolution Effects

R. S. Plant and B. W. Atkinson

Department of Geography
Queen Mary and Westfield College
University of London

Contents

Abstract

Phase 1 of this project was successful in simula ting the Marine Internal Boundary Layer (MIBL) resulting from the flow of hot, dry air from the Arabian/Kuwaiti landmass over the waters of the Gulf. The MIBL was associated with strong gradients of temperature, humidity and refractivity at both its top an   d its landward edge . Routine forecasts by the UK Meteorological Office use a horizontal grid length of about 15km whereas those used in Phase 1 were 6 km in length. It would be most useful if the results found in Phase 1 could be replicated in both qualitative and quantitative terms by a model with the coarser resolution used in routine procedures. This part of the work provided runs at different horizontal resolutions to assess their effects on the quality of the simulated features. A series of simulations was made with grid lengths of 3, 6, 9, 12 and 15km.

The results show that the description of the atmospheric environment was significantly enhanced in the fine resolution simulations. In the low   -wind cases, grid lengths as coarse as 15km could be used for   qualitative studies with little penalty, the location of a sea   -breeze front (SBF) and the depth of the MIBL remaining well represented. However, the runs at the smallest grid lengths captured not only the broad structures evident in all of the runs but al   so found stronger gradients in parts of the simulated features that may be critical to the propagation environment. These were evident, most notably, at the inversion at the top of the MIBL and across the land   -sea boundary. For the high-wind cases, even the qualitative description began to suffer at low resolution, as evidenced by the poor representations of uplift in the SBF.

The fine resolution runs revealed a perturbation in the depth of the MIBL that appeared to be related to the sea   -breeze circulation. It had a significant effect on the distribution of refractivity in the lowest 200m of the atmosphere.

3

1. **Introduction**

This project is concerned with assessing the capability of mesoscale numerical models for predicting the propagation environment in coastal areas. Phase 1 covered the testing of a non -hydrostatic, numerical model in idealised and realistic situations (Li and Atkinson 1997ab, 1998ab). The realistic cases (Li and Atkinson 1998b) were run to simulate conditions in the Persian Gulf in a p eriod when aircraft observations had been taken (Brooks et al. 1997, 1999). The results were encouraging and showed that the model was capable of capturing the essential features of the propagation environment. A marine boundary layer (MBL) over the Gulf w as well simulated in both its depth and the gradients of temperature, humidity and refractivity therein. In addition to the important vertical gradients at the top of the MBL, well   -developed sea -breeze circulations were found which exhibited a strong horiz ontal gradient at the boundary between sea and land air. It is tempting to call this gradient the sea   -breeze front (SBF), but care in nomenclature is required here as observations of such fronts show them to be hundreds of metres, rather than several kilom   etres, wide. The runs in Phase 1 had a horizontal resolution of 6km.

In the light of the results from Phase 1 it was decided to pursue four aspects of the project: first, the effects of horizontal grid resolution on the simulations; second, a more detailed analysis of the SBF; third, horizontal variations within the MBL; fourth, the incorporation of the TERPEM model, a code that allows calculation of the response of electromagnetic radiation to the propagation environment produced by the meteorological model. This report covers the effects of grid resolution.

2. **Model Configuration**

The horizontal grid length used in operational forecasts by the UK Meteorological Office is typically about 15km. It is therefore of interest to investigate the effects of different horizontal resolutions on the representation of the meteorological features found in Phase 1. This was done by performing two series of runs in the Gulf domain (Fig. 1)   - one for 'low wind' cases, the other for 'high wind' cases - in each of which the horizontal grid lengths were set to 3, 6, 9, 12 and 15km. (Note that the time step was left unchanged

throughout at 20s). The 'low' and 'high' categories of wind speed were those chosen by Brooks et al. (1997) to describe their observations. 'Low' wind speeds were about 5 m s^{-1} and 'high' wind speeds were about 15 m s^{-1}. Wind directions were from about 300 $^{\circ}$. In Sec. 3, the results are compared in the form of vertical cross -sections along an east -west line in the domain (Fig. 1). This is the same line a s was used for the comparison with the aircraft results of Brooks et al. (1997, 1999) in Li and Atkinson (1998b; also Atkinson and Li 1999).

The vertical grid structure and the boundary and initial conditions were almost identical to those of the real case runs of Phase 1. For completeness, these are briefly recalled in Sec 2.1 below. Some minor changes to the initial conditions have been made in attempt to reduce the time taken for the model to become fully adjusted to the initial specifications. These cha nges are highlighted and the effects on the model results are presented in Sec. 2.1.

2.1 Boundary and Initial Conditions

The model domain was located in the central part of the Persian Gulf, the origin of co -ordinates being at 51 °E 27 °N. The domain was 600km long in the east -west direction and 360km in the north -south direction, which placed the boundaries a significant distance from the main area of interest. Although the mesoscale model formulation was designed to be able to cope with the effects of or ography (Carpenter 1979), these were not considered to be significant in the present application. The shallow slope down towards the eastern coast of Arabia has been neglected, as well as the stronger slopes on the north -eastern coastline of the Persian Gu lf. Justification for the latter simplification arises from the fact that this area lies downwind from the region to be investigated. Conditions within the region of interest were thus unlikely to be significantly perturbed by the detailed behaviour in the north-eastern corner of the model domain.

The land surface was taken to be uniform, with surface parameters suitable for desert conditions (Li and Atkinson 1998b). Although perhaps one of the more questionable aspects of the mesoscale model, a constant se a-surface temperature was set throughout the Gulf waters. A value of 23 °C was chosen in Li and Atkinson (1998b)

based on aircraft measurements taken at midday during the SHAREM -115 observations (Brooks et al. 1997). However, Li and Atkinson (1998b) pointed out that, even assuming saturated vapour, the observed water -vapour mixing ratios implied a sea -surface temperature in excess of 24 °C. Recalling that the limited number of surface -temperature measurements are subject to an error of ±0.5°C (see Table 2 of Brooks et al. 1997), it did not seem unreasonable to increase the input temperature to 24°C in the present work.

As in Li and Atkinson (1998b), wind profiles were set from the synoptic conditions at intermediate heights, falling off linearly in the top few levels of the model and logarithmically towards the surface. There were 33 model levels, extending up to a height of 10km, with level spacing increasing with height to ensure adequate resolution at low altitudes. The actual settings can be found in Li and Atkinson (1998b). For a given vertical θ profile, the corresponding values for the initial pressure field were determined using the hydrostatic approximation, applying the method described in Li and Atkinson (1997b).

Initial profiles of relative humidity and of θ were chosen by Li and Atkinson (1998b) as a compromise between typical high and low -wind profiles reported by Brooks et al. (1997). This choice of initial conditions may have contributed to the differences between model results on the first and se cond days. In the present work, therefore, the initial profiles have been adjusted towards the predicted profiles from the simulations of Li and Atkinson (1998b). This reduced the time required for the model to adjust to the initial configuration. In Li and Atkinson (1998b), the profiles were:

$$R = \begin{matrix} 80 - 230z \\ 11.3 - z \end{matrix} \begin{cases} z \le 0.3 \\ z > 0.3 \end{cases}$$

$$\theta = \begin{matrix} 22.5 + 25z \\ 28.2 + 6z \end{matrix} \begin{cases} z \le 0.3 \\ z > 0.3 \end{cases}$$

where z is to be expressed in km, R as a percentage and θ in degrees Celsius. For the low wind cases, these have been changed to:

$$R = \begin{array}{l} 75 - 600z \\ 15.1 - z \end{array} \left. \begin{array}{l} z \le 0.1 \\ z > 0.1 \end{array} \right.$$

$$\theta = \begin{array}{l} 23.5 + 45z \\ 27.4 + 6z \end{array} \left. \begin{array}{l} z \le 0.1 \\ z > 0.1 \end{array} \right.$$

while the high wind cases have used the following:

$$R = \begin{array}{l} 75 - 200z \\ 15.3 - z \end{array} \left. \begin{array}{l} z \le 0.3 \\ z > 0.3 \end{array} \right.$$

$$\theta = \begin{array}{l} 22.5 + 15z \\ 22.8 + 12z \\ 27 + 5z \end{array} \left. \begin{array}{l} z \le 0.1 \\ 0.1 < z \le 0.6 \\ z > 0.6 \end{array} \right.$$

One further change from the configuration used by Li and Atkinson (1998b) concerned the outgoing wave speed used in the radiative boundary condition of normal horizontal velocity. For the high wind runs only, this was increased from 10m s^{-1} (see Li and Atkinson 1997a) to 15m s^{-1}.

The changes noted above were made to reduce spin up time and do not alter any of the general qualitative conclusions drawn in Li and Atkinson (1998b; Atkinson and Li 1999). As expected, after the changes the model profiles of potential temperature and water vapour were established much more quickly so that the model results were more reliable at earlier times. There was also less difference observed between the model results on the first and second days. During the daytime, it was found that, after the changes, the mixing layer over the sea was slightly shallower and ~1°C warmer. Moreover, the transition between this mixed layer and the stable layer above occurred over a smaller distance, leading to somewhat stronger vertical gradients of water vapour and potential temperature at the top of the MBL. The night-time surface duct was observed to be stronger over land but weaker over the sea, and shallower throughout. This was undoubtedly caused by changes to the vertical gradients of water vapour and led to more variation of the low-altitude profiles in the horizontal. By contrast, the night-time temperatures over ground were in fact slightly greater and marginally weakened the duct.

7

3. **Results**

It is both convenient and instructive to compare the results in the form of vertical cross-sections extending west-east across the domain. Further it is useful to categorise the results into low wind and high wind cases as did Brooks et al. (1997) in their observations and as done in Phase 1. The detailed comparisons are reported for 1400hr local time[1] along a line 54km to the south of the domain centre[2]. The various runs are identified as follows: runs with horizontal grid length of 3km are called $\Delta 3$; those with 6km as $\Delta 6$ and so on.

3.1 Low Wind Cases

Several general points can be made before detailed comparison of individual elements. First, the model profiles evolved faster at the finer resolutions. Second, there was more difference between the results of the first and second days at finer resolution. This is a slightly curious observation but could be related to the point made by Brooks et al. (1997, 1999) that standard parameterizations may not be wholly suitable for stable atmospheric conditions over a sea surface. It seems reasonable to suppose that any defects in the model parameterizations could be exaggerated by the finer resolutions. Third, although weaker in these cases, the nocturnal SBF penetrated somewhat further inland at the degraded resolutions, almost reaching the western domain boundary in $\Delta 12$ and $\Delta 15$. Bearing in mind the forcing of sea breezes it is perhaps a little surprising that they exist at night but observations show this to be the case (Buckley and Kurzeja 1997). The model captures this phenomenon but the simulations at the coarser resolution may have allowed the sea breeze to penetrate too far inland. Fourth, the night-time land temperatures were slightly lower at fine resolution, but the temperatures at higher

---

[1] Complete write ups of all model data were performed less frequently for the $\Delta 3$ runs (every 3 hours) than at other resolutions (every 2 hours) since the large volume of data would otherwise have caused a crash due to the disk limits on the machine then being used. This has entailed that the plots shown in this report for $\Delta 3$ are in fact at 1500hr local time. Inspection of the frequent partial write ups indicates that conditions changed only slowly between 1400 and 1500hr. Moreover, since there are several plots available at 1400hr with which to identify or confirm trends in the sensitivity to resolution, we believe that this time difference for the $\Delta 3$ plots is not sufficient to invalidate any of the general points we have made.

[2] For resolutions where there were no grid points along that line, the closest grid line to the stated position was chosen instead.

altitudes were a little higher. Also, the minimum night-time surface temperatures persisted for longer as the resolution increased. Finally, a nocturnal jet over the sea was strongest for intermediate resolutions, such as $\Delta9$.

3.1.1 Temperature

The cross-sections of temperature are shown in Fig. 2. Superficially the figures look very similar but closer inspection reveals significant differences. It is easiest to identify them by contrasting the results for $\Delta3$ with those for $\Delta15$. The boundary between the marine and land air was more sharply represented in $\Delta3$ than in $\Delta15$ (compare the configuration of isotherms for 30 to 32 ^{o}C at about $x = -80$ to -90km in Figs. 2a and 2e). The inversion at the top of the MBL was stronger in $\Delta3$ than in $\Delta15$. In $\Delta3$ (Fig. 2a) the temperature change from 25 to 27 ^{o}C generally occurred between ~60 and ~80m, whereas in $\Delta15$ (Fig. 2e) the same temperature change occurred between ~40 and ~80m. It is difficult to make a detailed comparison with the aircraft observations (Brooks et al. 1997, 1999) because of the small vertical distances involved but the stronger vertical gradient captured by the $\Delta3$ run accords with previous results (Arya 1988, Stull 1988, Garratt 1992).

3.1.2 Vapour pressure

The cross-sections of vapour pressure at different resolutions (Fig. 3) again show much similarity, but three important differences were identified. First, a 'triangle' of values over 8mb can be seen in Fig. 3a lying between about -180 and -60km on the x-axis and extending up to about 400m. This feature appeared on all of the sections but was most pronounced in the $\Delta3$ case (Fig. 3a). The cause of this feature is not immediately obvious but it may be related to the incursion and subsequent uplift of marine air over the land due to the sea breeze (see Fig. 5). Second, there were differences in the land-sea gradient of vapour pressure at the head of the sea breeze, due to resolution. At $\Delta3$, the transition from 10 to 20mb occurred over a distance of ~15km whereas in the $\Delta15$ case (Fig. 3e) it occurred over a distance of ~40km. Consequently the horizontal gradient in the finest resolution case may be as much as three times stronger than with the coarsest

resolution. Third, the vertical gradient of vapour pressure at the top of the MBL was strongest in the Δ3 case. This increase existed because, although the height of the 10mb line was the same in all cases, in the Δ3 case (Fig. 3a) the 20mb line was higher than in, for example, the Δ15 case (Fig. 3e).

3.1.3 Refractivity

The cross sections of refractivity (Fig. 4) reflect those of humidity. The strengths of the vertical gradients a t the top of the MBL and the horizontal ones across the SBF were greatest in the Δ3 case (Fig. 4a). The relative strengthening was again due to the base of the capping inversion being higher in the   Δ3 case than in the cases with longer grid lengths, wherea s the top of the inversion was virtually the same across the range of grid lengths. If this configuration is turned anti   -clockwise through 90 ^{o} it also gives the essence of the land   -sea contrast, albeit with the latter extending over much greater horizontal distances than the vertical distances involved in the capping inversion.

At high altitudes (above 300m or so) moving from west to east, the isolines of refractivity dipped at the coast before undergoing a net rise. Although it seems unlikely that such a horizontal structure would significantly modify a radar signal, it is interesting to note that the dip was better captured at finer resolution, presumably being correlated to the presence of the SBF.

3.1.4 Wind

Cross sections of the wind field are shown   in Fig. 5. The most striking feature in all the runs was the uplift occurring over the coastline associated with the sea breeze. At Δ3 the uplift was strong and, at $x = -80$km, vertical, reaching heights of about 800m (Fig. 5a). Downwind of this feature subsidence occurred over the upper 600m or so of the layer occupied by the sea breeze circulation. The line of sign reversal between the sea   -breeze current itself and the overlying return current lay at about 200m near the front, decreasing in height until it was virtually at the surface about 100km downwind at $x \sim 0$km. In the Δ15 case (Fig. 5e), although the location of the SBF was virtually identical to that seen in Fig. 5a, the uplift associated with it was not as clearly vertical. The whole sea   -breeze circulation was weaker, more tilted downwind and shallower than in the Δ3 run.

10

3.2 High Wind Cases

Several general points can again be made before detailed comparison of individual elements. First, there were some indications of horizontal undulations in the isolines of refractivity at the highest resolution (see Fig. 8e, at around x=80km and x=240km). Second, more water vapour was found over land at the higher resolutions, probably due to the improved capture of a SBF. Third, there was more difference between the first and second days as the resolution increased (see Sec. 3.1.5). Fourth, the nocturnal MBL was deeper at high resolution. Finally, the surface energy budgets suggest that cloud formation occurred in these high wind runs over the sea (see, for exam ple, Fig. 17b of Li and Atkinson 1998b). This began at around 0800hr and was much more pronounced at higher resolution, disappearing almost entirely in Δ15.

3.2.1 Temperature

Cross sections of simulated temperature in the high wind cases are shown in Fig. 6. As the resolution varied, the main difference was in the representation of the boundary between the sea and land air. In Δ15 (Fig. 6e) the zone was wide, temperatures changing from 32°C to 25°C over a distance of ~150km. In the Δ3 case (Fig. 6a) the s ame change occurred over about 90km, and the change 32°C to 26°C over a distance of ~60km. As well as capturing the greatest horizontal gradient, the Δ3 run also revealed steeply sloping isotherms, in contrast to the runs with coarser resolution but in ac cord with observations of sea -breeze structure. Associated with the land -sea boundary in Δ3 was a tongue of warm air at a height of ~400m, reaching eastwards to about x =100km (Fig. 6a). Such a feature also appeared in runs Δ6, Δ9 and Δ12 but was lower (ab out 300m) and reached only to ~60km. In run Δ15 (Fig. 6e) the tongue reached out to ~90km but was again shallower than in Δ3 (Fig. 6a).

3.2.2 Vapour pressure

If defined by the vapour pressure, the depth of the MBL was about 350m in all runs, but a litt le deeper at the highest resolution (Fig. 7a). Using large grid lengths the

isolines were smooth and fairly evenly spaced. In the run $\Delta 9$ (Fig. 7c) a perturbation occurred on the top of the MBL, best seen in the 8mb isoline, and a similar feature was evident in $\Delta 3$ (Fig. 7a) in the 10mb isoline around $x = 0$km. This feature bears a resemblance to the configuration of velocity associated with the vertical overturning at the SBF (see Simpson 1994) but it is premature to link the two at this stage.

3.2.3 Refractivity

Cross sections of refractivity are shown in Fig. 8. Comparison is facilitated by concentrating on the $\Delta 3$ and $\Delta 15$ runs. Higher values of M over the sea occurred in $\Delta 3$ than in $\Delta 15$, causing a deeper layer of inverted M in the former case (~ 410m in $\Delta 3$; ~ 370m in $\Delta 15$). Associated with the deeper layer in $\Delta 3$ was a slightly stronger lapse of M at the top of the MBL. Horizontal gradients also differed between the runs. In $\Delta 15$ they were fairly uniform over the distance -100 to 0km, whereas the same refractivi ty change occurred over ~ 60km in $\Delta 3$, with more steeply sloping isolines.

3.2.4 Wind

Cross sections of wind are shown in Fig. 9. Significant differences were apparent as the resolution varied. In the $\Delta 3$ case (Fig. 9a) quite marked uplift occurred between $x = -72$ and -24km, extending up to ~ 1km. Also, the flow took on a downward component beyond about $x = 24$km. The sea -breeze current itself produced no flow counter to the direction of the ambient wind but air was almost stationary at the first two levels at $x = -36$km, showing the effect of the breeze. Fig. 9a shows that the convergence and uplift zone at the head of the sea breeze was shifted ~ 20km offshore by the ambient winds, a position that coincided with the marked horizontal gradients of temperature and humidity. Comparison of the distributions of wind (Fig. 9a) and humidity (Fig. 7a) shows that the uplift at the SBF was able to take moist air up to a height of 800m, as shown by the 'tongue' of the 8mb isoline. Downwind of $x = 60$km the MBL was about 400m d eep, probably being constrained by larger scale subsidence. In contrast to the above organisation of the wind field, the $\Delta 15$ case (Fig. 9e) showed no clear uplift.

12

4. Structure of the MBL

In Sec. 3, the effects of horizontal grid resolution on the propaga tion environment that was described by Li and Atkinson (1998b) have been discussed. In the present section, attention is drawn to a feature of potential importance, seen most clearly in the high-resolution Δ3 run performed for low winds (Fig 2). Once ident ified, hints of the same structure could be found at coarser resolution and also in the high wind case. Investigation of the feature is aided by a consideration of the behaviour of internal boundary layers (IBLs).

"Internal boundary layers in the atmospher e are associated with the horizontal advection of air across a discontinuity in some property of the surface" (Garratt 1990, p171). In the present case the flow was from a hot, dry surface over the cool, wet one of the Gulf. This resulted in a cool, stable and moist MBL which is at the same time a stable IBL, giving rise to the nomenclature Marine Internal Boundary Layer (MIBL). The growth of IBLs in general is a major component in their analysis. The growth of stable IBLs has been addressed by, among other s, Garratt (1987), Garratt and Ryan (1989), Hsu (1983) and Mulhearn (1981). Garratt (1987) proposed the following relation

$$ h^2 = \alpha^2 U^2 \left(\frac{g \Delta \theta}{\theta} \right)^{-1} x $$

where h is the IBL height (m), U is the geostrophic wind component perpendicular to the coast (m s^{-1}), x is the fetch (km) and $\Delta\theta$ is the difference between the potential temperatures over land and at the sea surface. Garratt (1987) originally proposed a value for α of 0.014, very similar to Mulhearn's (1981) value of 0.015. However, after an observational programme, Garratt and R yan (1989) concluded that these values were too small, suggesting a value of 0.024 and recognising that the magnitude of the coefficient was variable. The value appropriate for the MIBLs in these simulations is ~0.03. Using this value, the uninterrupted gr owth of the simulated MIBL over the first 140km downwind of the coast in the Δ3 case would be as shown in Fig. 10. In fact, over the first 90km or so the simulated MIBL did not grow in accord with theory, a step -like feature being manifest instead (Fig. 10 , and see the θ =28°C line in Fig . 2a, the q=8mb line in

13

Fig. 3a and the M=295 line in Fig. 4a). At a distance of about 40km downwind the growth rate fell to zero or even negative values (a slight decrease in the MIBL height occurred along the step). At about 90km the growth rate increased sharply to give a depth of the MIBL in accord with the theory.

A feature bearing some resemblance to the perturbation noted above can be found in the numerical modelling of Garratt (1987). In that paper a jump in the MIB L height was associated with an increase in air temperature over land at sunrise: the jump occurred where the rapidly heated land air met the cool air in the MIBL. The jump structure moved further out to sea at later times as the air was advected downstrea m. Such a mechanism can be ruled out in the present case, since the jump structure remained static, its location being very strongly linked to that of the SBF. Moreover, the jump from the flat portion occurred around x~0, the fetch at which the wind becam e offshore for all heights. This suggests that the structure schematically shown in Fig. 10 arose from an interaction of the sea-breeze circulation and the MIBL. This phenomenon will be further investigated in the next stage of this project.

5. **Conclusion**

Phase 1 of this project was successful in simulating the MIBL resulting from the flow of hot, dry air from the Arabian/Kuwaiti landmass over the waters of the Gulf. The MIBL was associated with strong gradients of temperature, humidity and refractivity at both its top and its landward edge . Routine forecasts by the UK Meteorological Office use a horizontal grid length of about 15km whereas those used in Phase 1 were 6km in length. It would be most useful if the results found in Phase 1 could be replicate d in both qualitative and quantitative terms by a model with the coarser resolution used in routine procedures. This part of the work provided runs at different horizontal resolutions to assess their effects on the quality of the simulated features. A seri es of simulations was made with grid lengths of 3, 6, 9, 12 and 15km.

The results show that the description of the atmospheric environment was significantly enhanced in the fine resolution simulations. In the low -wind cases resolutions as coarse as $\Delta15$ could be used for qualitative studies with little penalty, the location of an SBF and the depth of the MIBL remaining well represented. However, the runs at the smallest grid lengths captured not only the broad structures evident in all of

14

the runs but also f ound stronger gradients in parts of the simulated features that may be critical to the propagation environment. These were evident, most notably, at the inversion at the top of the MIBL and across the land -sea boundary. Noonan and Smith (1986) presented a similar finding. For the high -wind cases, even the qualitative description began to suffer at low resolution, as evidenced by the poor representations of uplift in the SBF (see Fig. 9).

The fine resolution runs revealed a perturbation in the depth of the M IBL that appeared to be related to the sea -breeze circulation. It had a significant effect on the distribution of refractivity in the lowest 200m of the atmosphere.

References

Atkinson, B. W. and J-G. Li 1999, Numerical modelling o f the propagation environment in the atmospheric boundary layer over the Persian Gulf. Submitted to *J. Appl. Metorol*.

Arya, S. P. 1988, *Introduction to micrometeorology*. Academic Press, 307pp.

Brooks, I. M., D. P. Rogers and A. K. Goroch 1997, SHAREM   -115 Observations: Atmospheric Environmental Assessment Data Collected by the UK Meteorological Research Flight C   -130 Hercules Aircraft, unpublished report (available from ftp://megan.ucsd.edu/pub/sharem), 53pp.

Brooks, I. M., A. K. Goroch and D. P. Rogers 1999, Observations of strong surface radar ducts over the Persian Gulf. *J. Appl. Meteorol.,* **38**, 1293-1310.

Buckley, R. L. and R. J. Kurzeja 1997, An observational study of the nocturnal sea breeze. Part 1: Structure and circulation. *J. Appl. Meteorol*., **36**, 1577-1598.

Carpenter, K. M. 1979, An experimental forecast using a non   -hydrostatic mesoscale model. *Quart. J. R. Meteorol. Soc*., **105**, 629-655.

Garratt, J. R. 1987, The stably stratified internal boundary   layer for steady and diurnally varying offshore flow. *Bound. Lay. Meteorol*. **38**, 369-394.

Garratt, J. R. 1990, The internal boundary layer   – A review. *Bound. Lay. Meteorol* ., **50**, 171-203.

Garratt, J. R. 1992, *The atmospheric boundary layer*. Cambridge University Press. 316pp.

Garratt, J. R. and B. F. Ryan 1989, The structure of the stably stratified internal boundary layer in offshore flow over the sea. *Bound. Lay. Meteorol*., **47**, 17-40.

Hsu, S. A. 1983 On the growth of a thermally modified boundary layer   by advection of warm air over a cooler sea*. J. Geophys. Res*., **88** (C1), 771-774.

Li, J-G. and B. W. Atkinson 1997a, Numerical modelling of the propagation environment in the atmospheric boundary layer over coastal areas: Literature review and mesoscale model. *Report No. 1, MoD Agreement No NNR/2042/1*, 36pp.

Li, J-G. and B. W. Atkinson 1997b, Numerical modelling of the propagation environment in the atmospheric boundary layer over coastal areas: Model sensitivity study. *Report No. 2, MoD Agreement No NNR/2042/1,* 69pp.

Li, J-G. and B. W. Atkinson 1998a, Numerical modelling of the propagation environment in the atmospheric boundary layer over coastal areas: Idealised case study . *Report No. 3, MoD Agreement No NNR/2042/1,* 65pp.

Li, J-G. and B. W. Atkinson 1998b, Numerical modelling of the propagation environment in the atmospheric boundary layer over coastal areas: Real case study – The Persian Gulf. *Report No. 4, MoD Agreement No NNR/2042/1,* 42pp.

Mulhearn, P. J. 1981, On the formation of a stably stratified internal boundary layer by advection of warm air over a cooler sea. *Bound. Lay. Meteorol*., **21**, 247-254.

Noonan, J. A. and R. K. Smith 1986, Sea breeze circulations over Cape York Peninsula and the generation of Gulf of Carpenteria cloud line disturbances, *J. Atmos. Sci.* , **43**, 1679-1693.

Simpson, J. E. 1994, *Sea breeze and local winds*. Cambridge University Press, 234pp.

Stull, R. B. 1988, *An introduction to boundary layer meteorology* . Kluwer Academic Publishers. 666pp.

Figure captions

Figure 1: Location of the SHAREM -115 area and the model domain. The boundaries are marked by broken and by solid lines respectively.

Figure 2: Cross-sections of temperature (°C) at 1400hr for the low wind cases. Sub-figure (a) is the cross-section obtained from the run with a 3km grid length; sub-figure (b) is that obtained using a 6km grid length; sub -figure (c) is that obtained using a 9km grid length; sub-figure (d) is that obtained using a 12km grid length; and sub -figure (e) is that obtained using a 15km grid length. As noted in the main text, the sub -figure (a) results are for 1500hr local time whereas all other results are for 1400hr local time.

Figure 3: Cross -sections of vapour pressure (mb) at 1400hr for the low wind cases. The sub-figures (a) to (e) have the same meaning as in Fig. 2.

Figure 4: Cross -sections of refractivity (M units) at 1400hr for the low wind cases. The sub-figures (a) to (e) have the same meaning as in Fig. 2.

Figure 5: Cross-sections of the wind at 1400hr for the low wind cases. The sub-figures (a) to (e) have the same meaning as in Fig. 2. The u component of the wind is plotted in units of m s $^{-1}$ and the w component in units of cm s $^{-1}$. The scale for the u component is provided by a reference arrow representing 2 m s $^{-1}$ shown at a hei ght of 610m and x $\sim$ -300km; that for the w component is provided by a reference arrow representing 2 cm s $^{-1}$ shown at a height of 460m and x ~ -300km.

Figure 6: Cross -sections of temperature at (°C) 1400hr for high wind cases. The sub - figures (a) to (e) have the same meaning as in Fig. 2.

Figure 7: Cross-sections of vapour pressure (mb) at 1400hr for high wind cases. The sub - figures (a) to (e) have the same meaning as in Fig. 2.

Figure 8: Cross-sections of refractivity (M units) at 1400hr for high wind ca ses. The sub- figures (a) to (e) have the same meaning as in Fig. 2.

Figure 9: Cross-sections of the wind at 1400hr for high wind cases. The sub-figures (a) to (e) have the same meaning as in Fig. 2. The scales are as in Fig. 5.

Figure 10: A semi-schematic diagram of the perturbation in the marine internal boundary layer (MIBL). The solid line shows the evolution of the MIBL height downstream, as predicted by theoretical relation. The dotted line illustrates the evolution predicted from the numerical mesoscale model.

Fig.1 Location of SHAREM-115 area (- - -) and model domain (—).
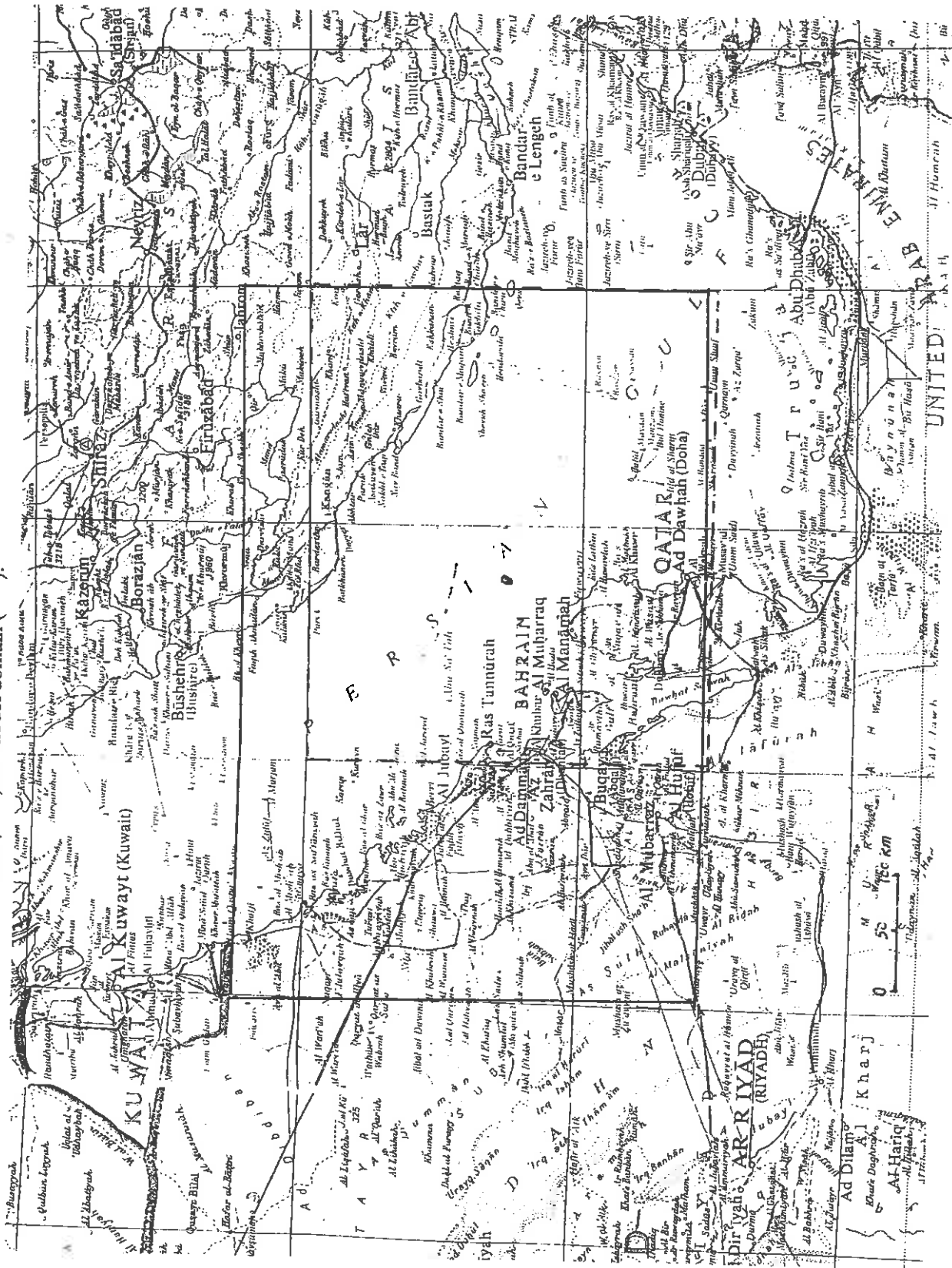
Fig 2a. Temperatures (C) along Y=-54km at 1500 with 3km grid length
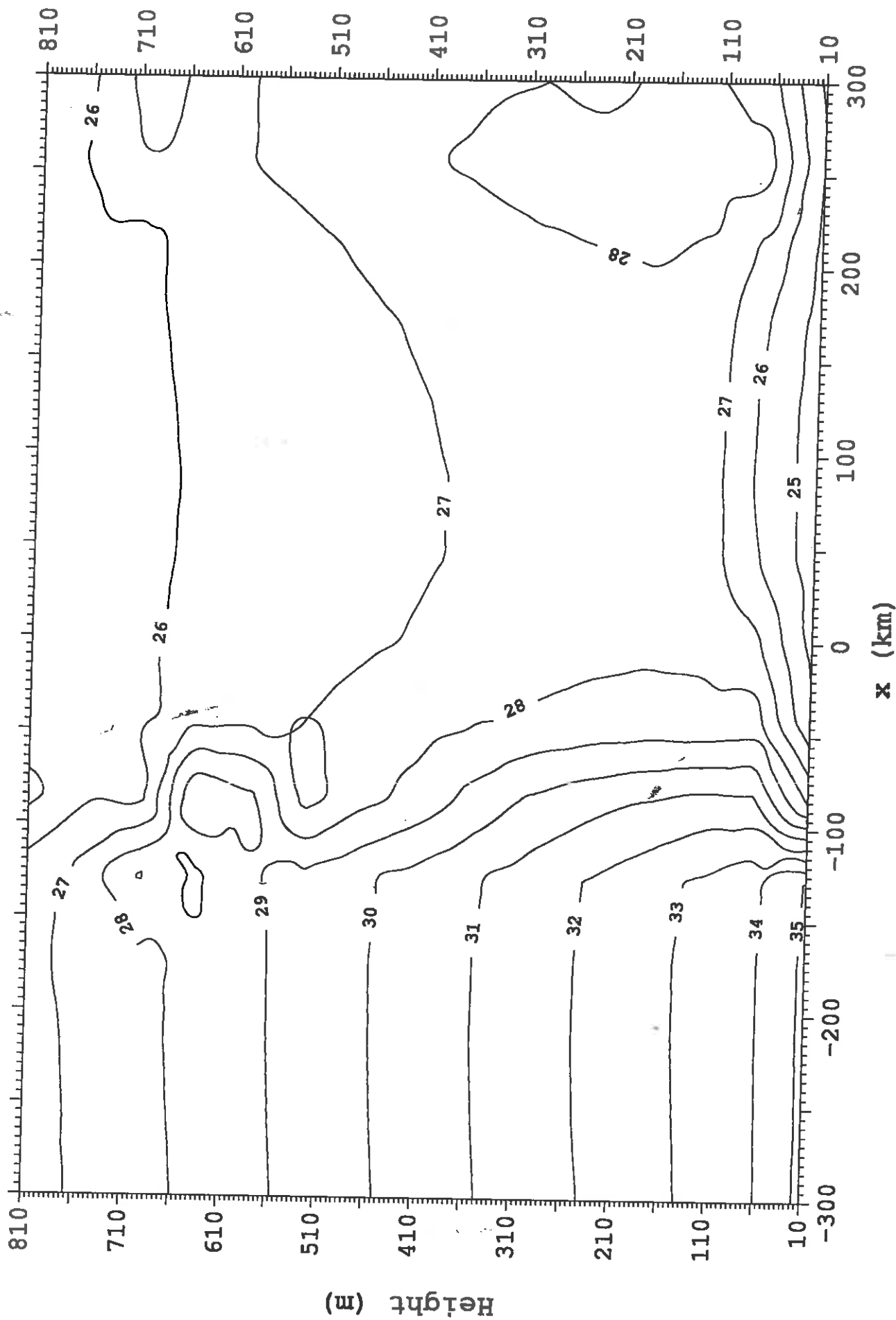
Fig 2b. Temperatures (C) along Y=-54km at 1400 with 6km grid length
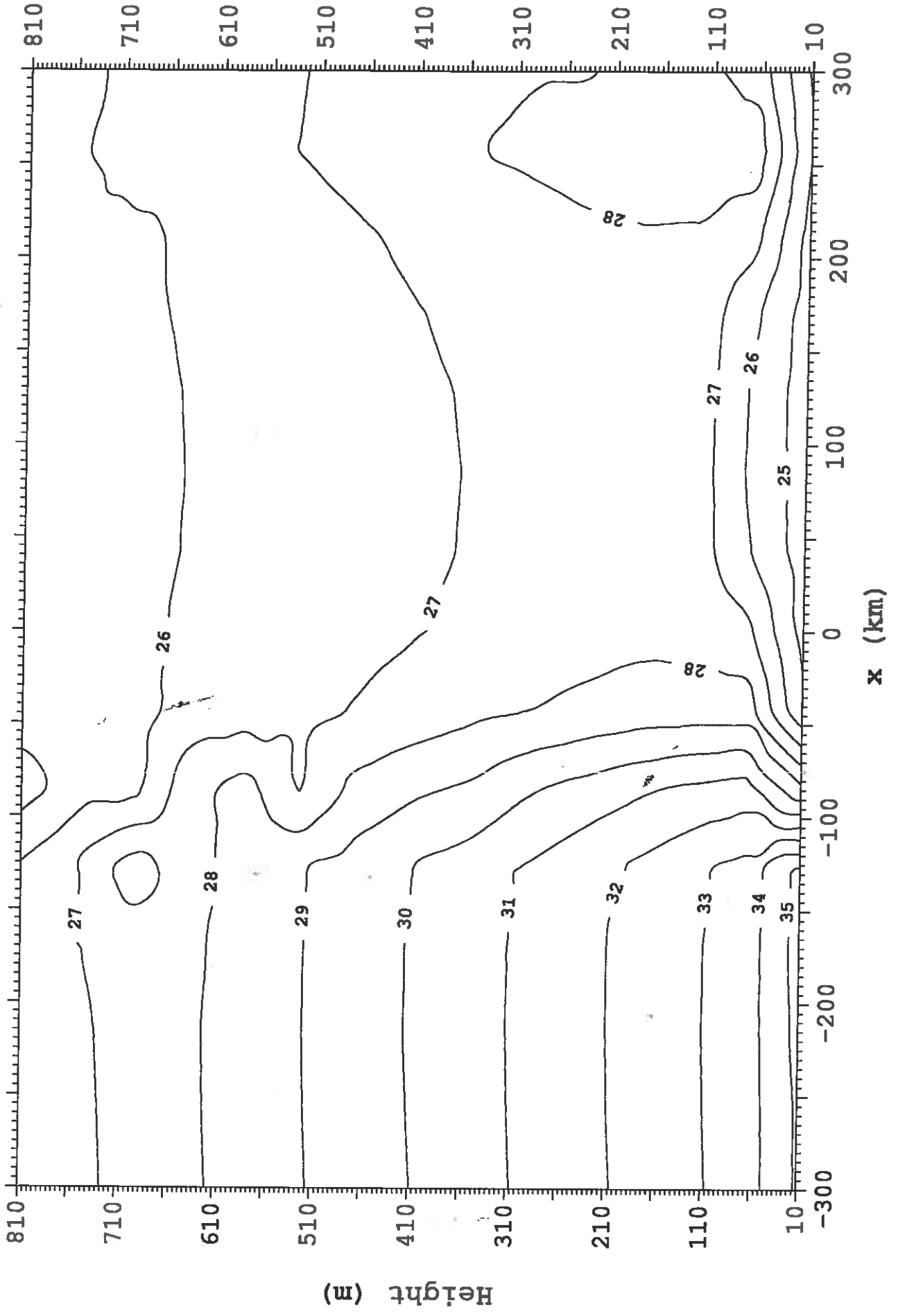
Fig 2c. Temperatures (C) along Y=-54km at 1400 with 9km grid length
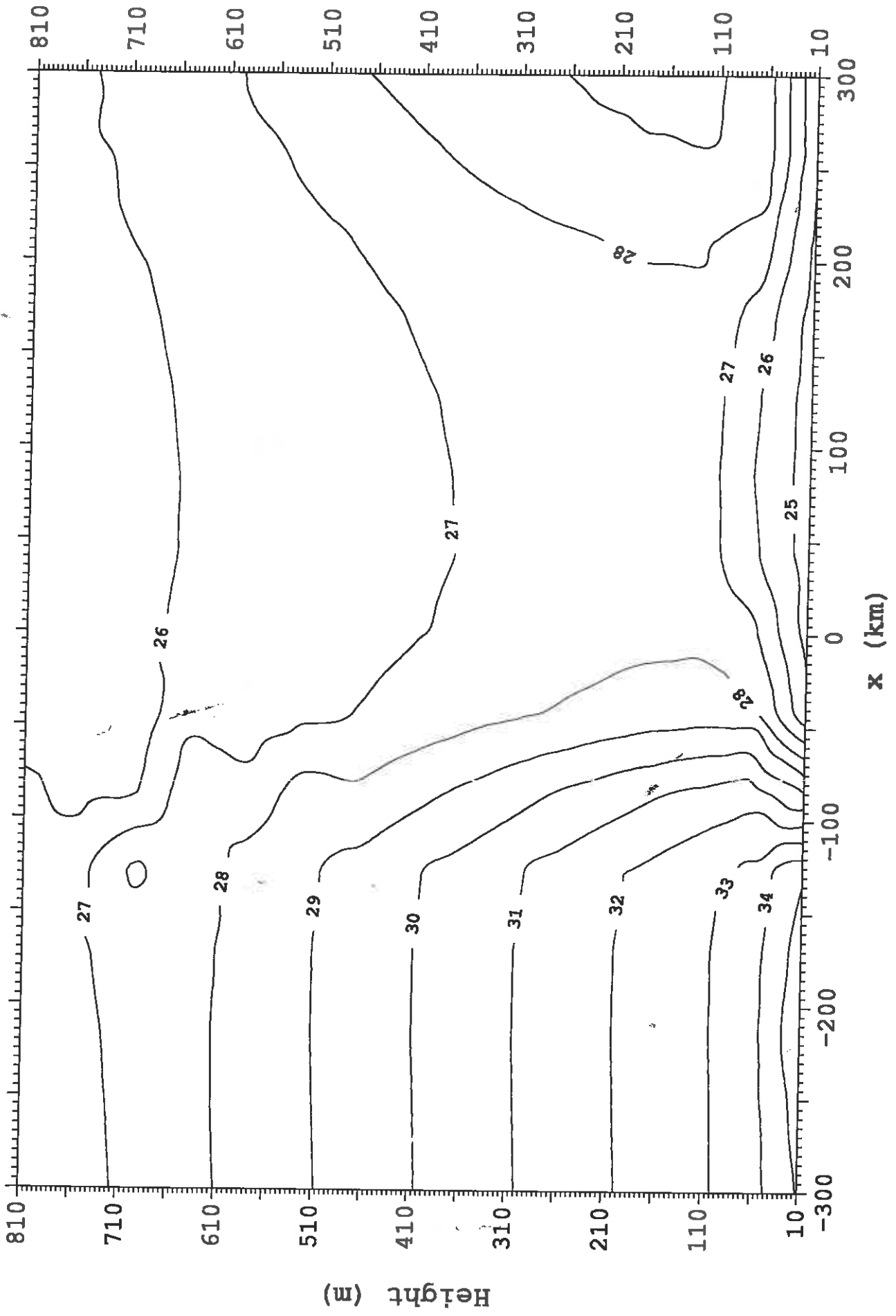
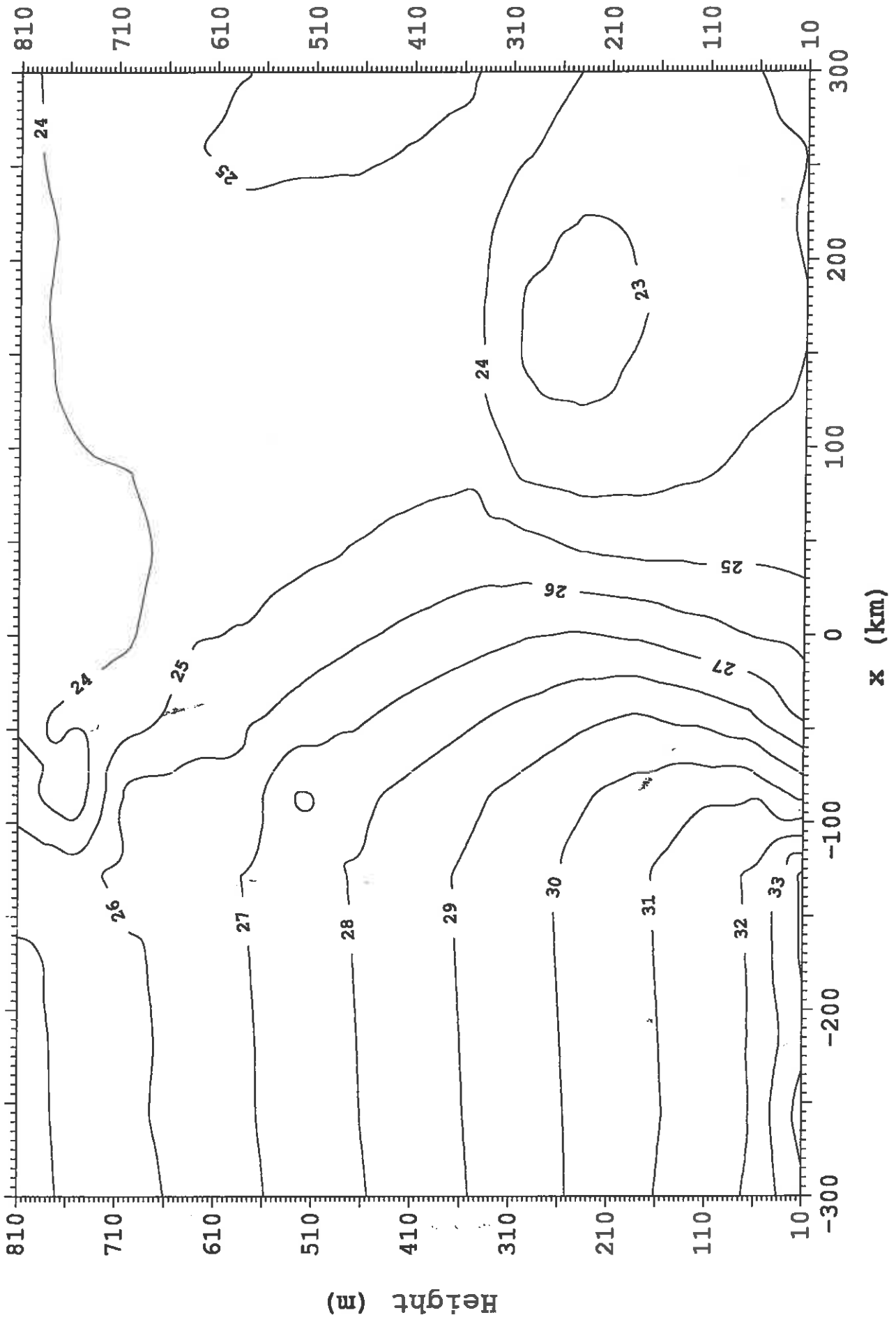Fig 2d. Temperatures (C) along Y=-54km at 1400 with 12km grid length
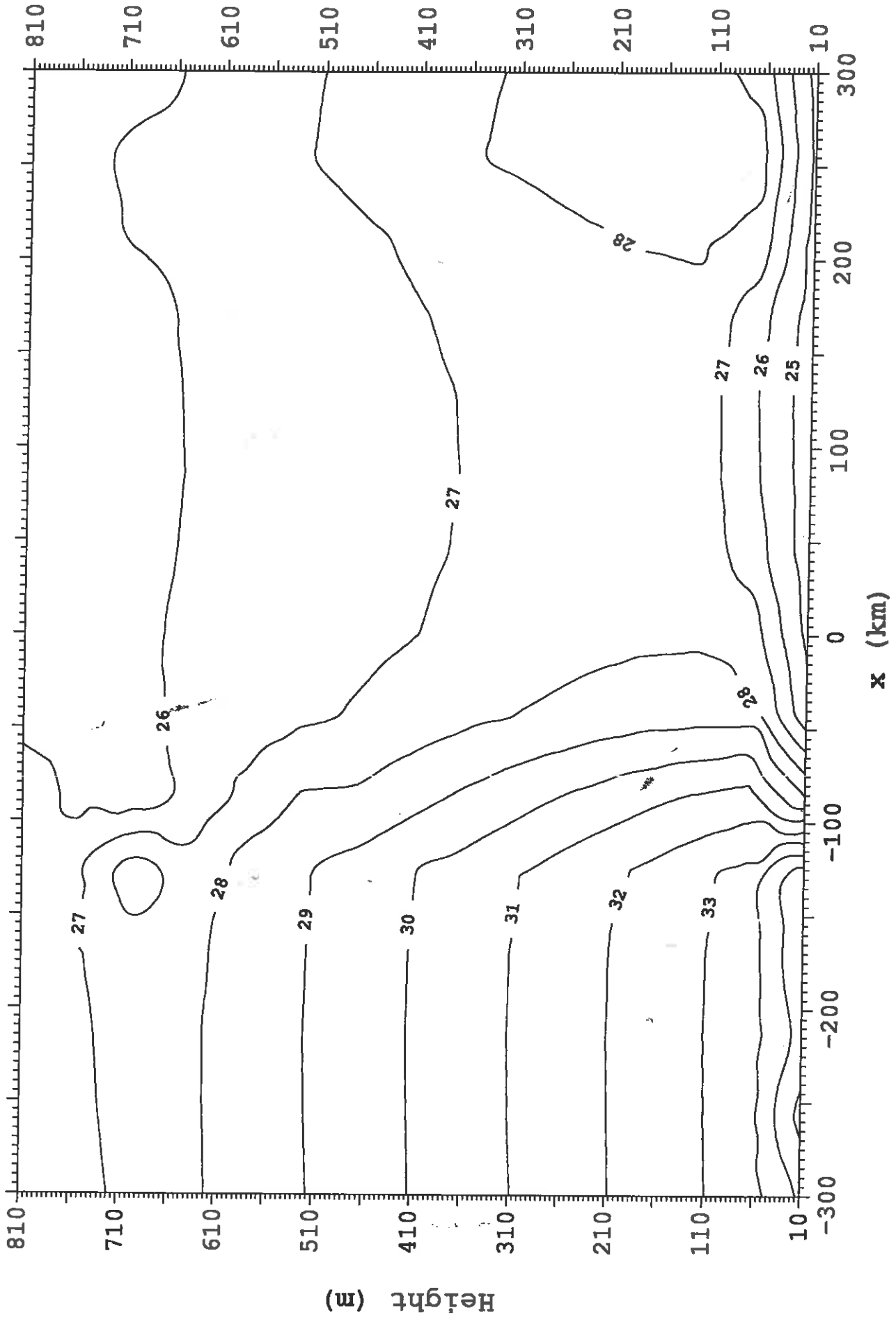
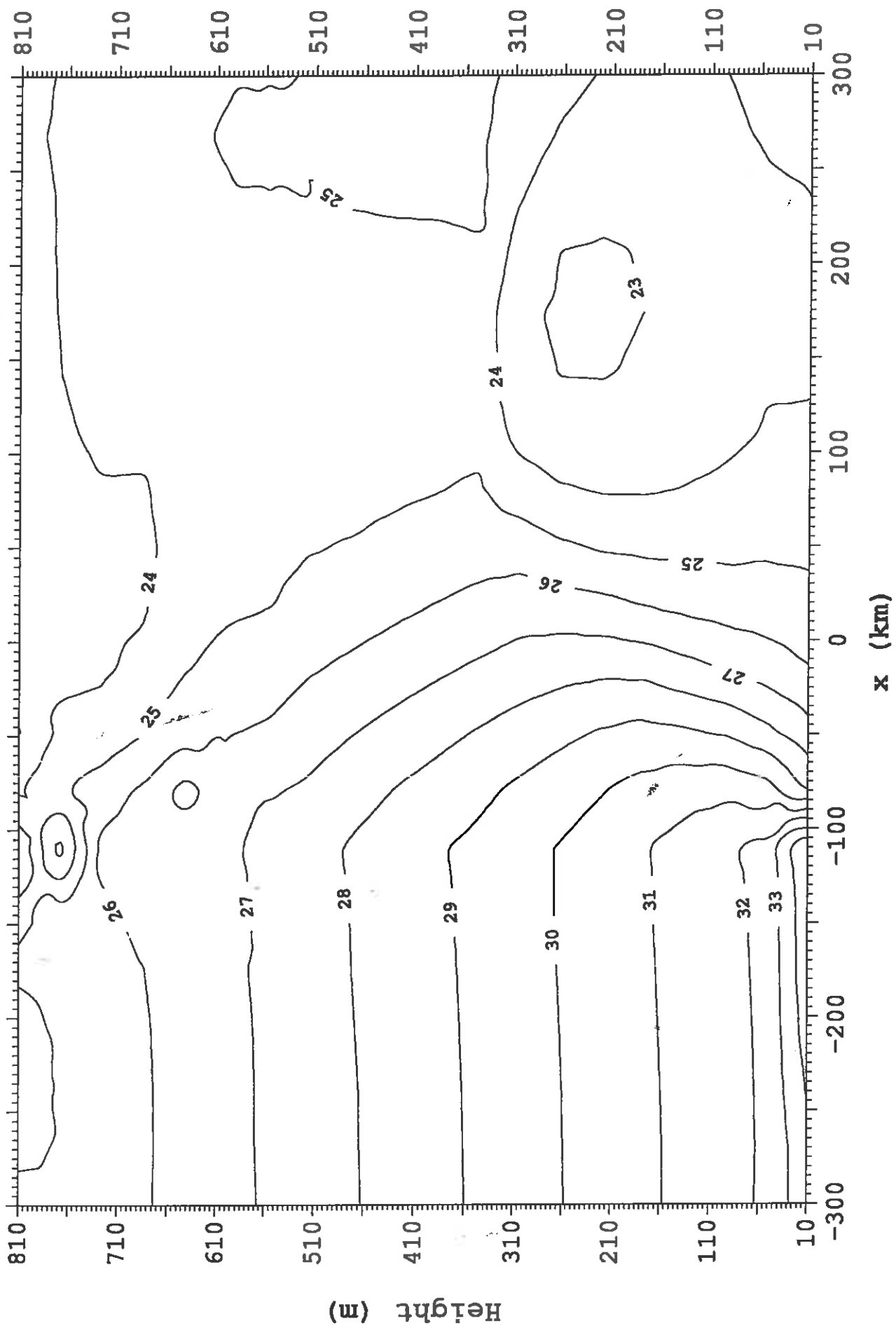Fig 2e. Temperatures (C) along Y=-54km at 1400 with 15km grid length
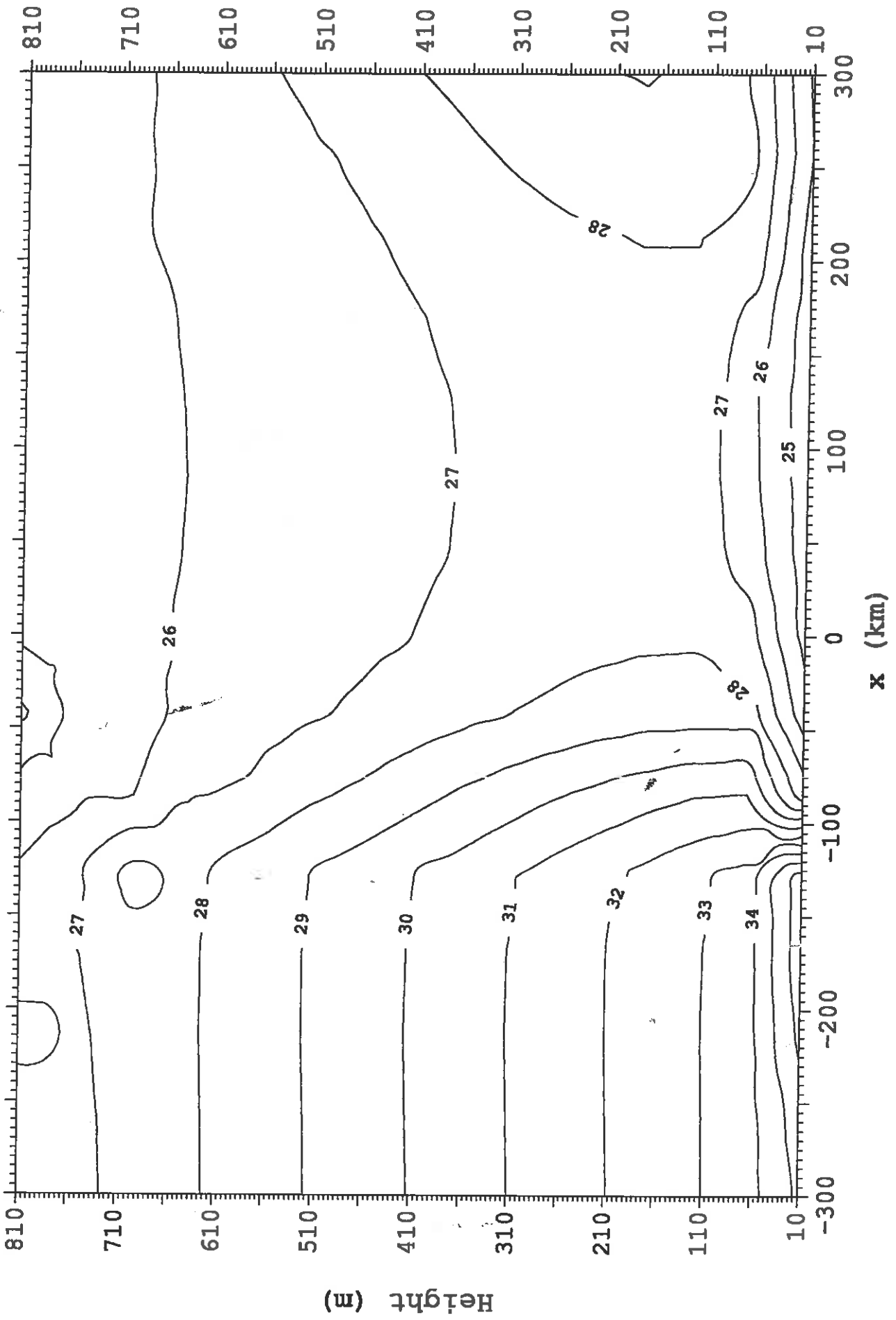
Fig 3a. Vapour pressure (mb) along Y=-54km at 1500 with 3km grid length
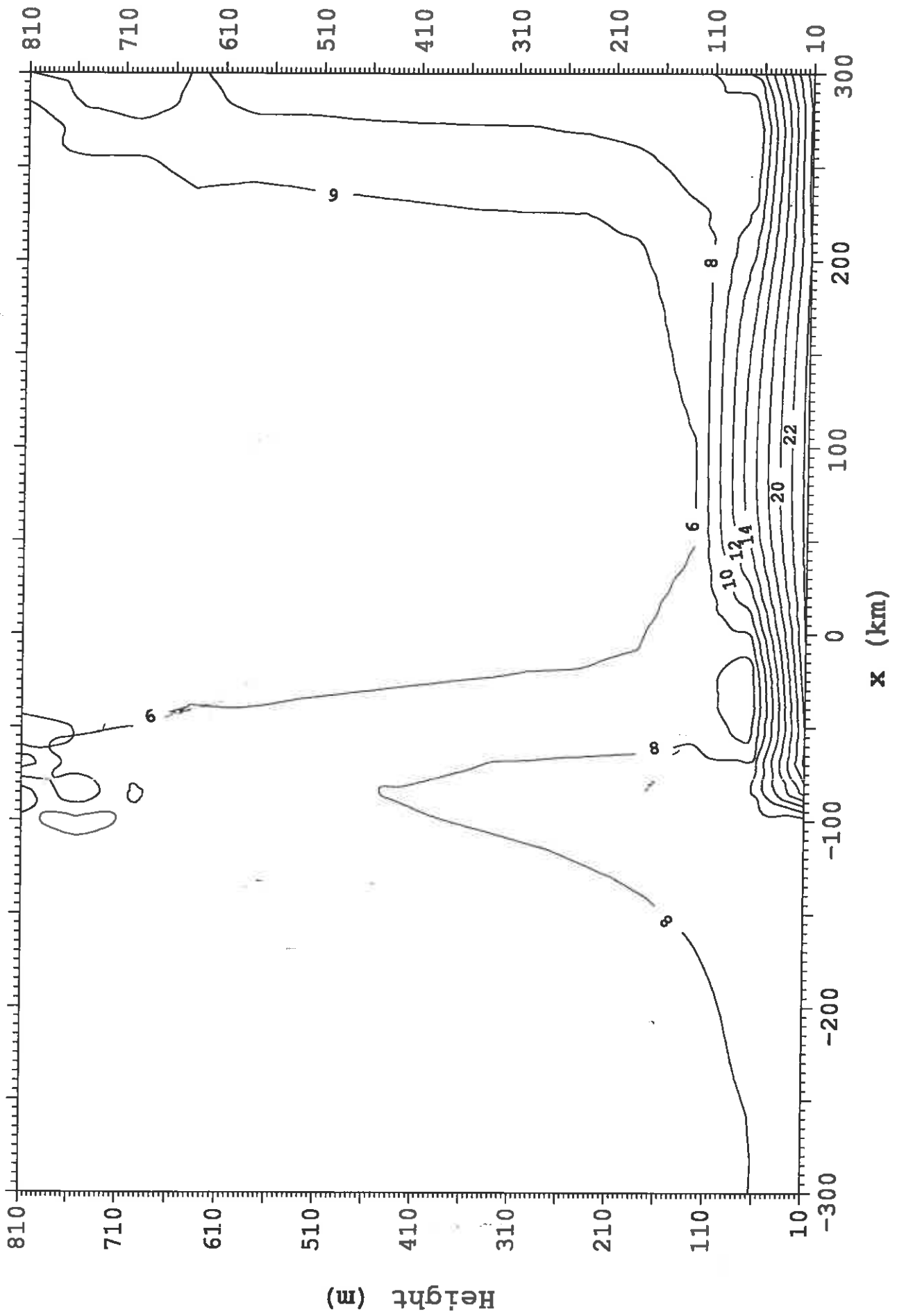
Fig 3b. Vapour pressure (mb) along Y=-54km at 1400 with 6km grid length
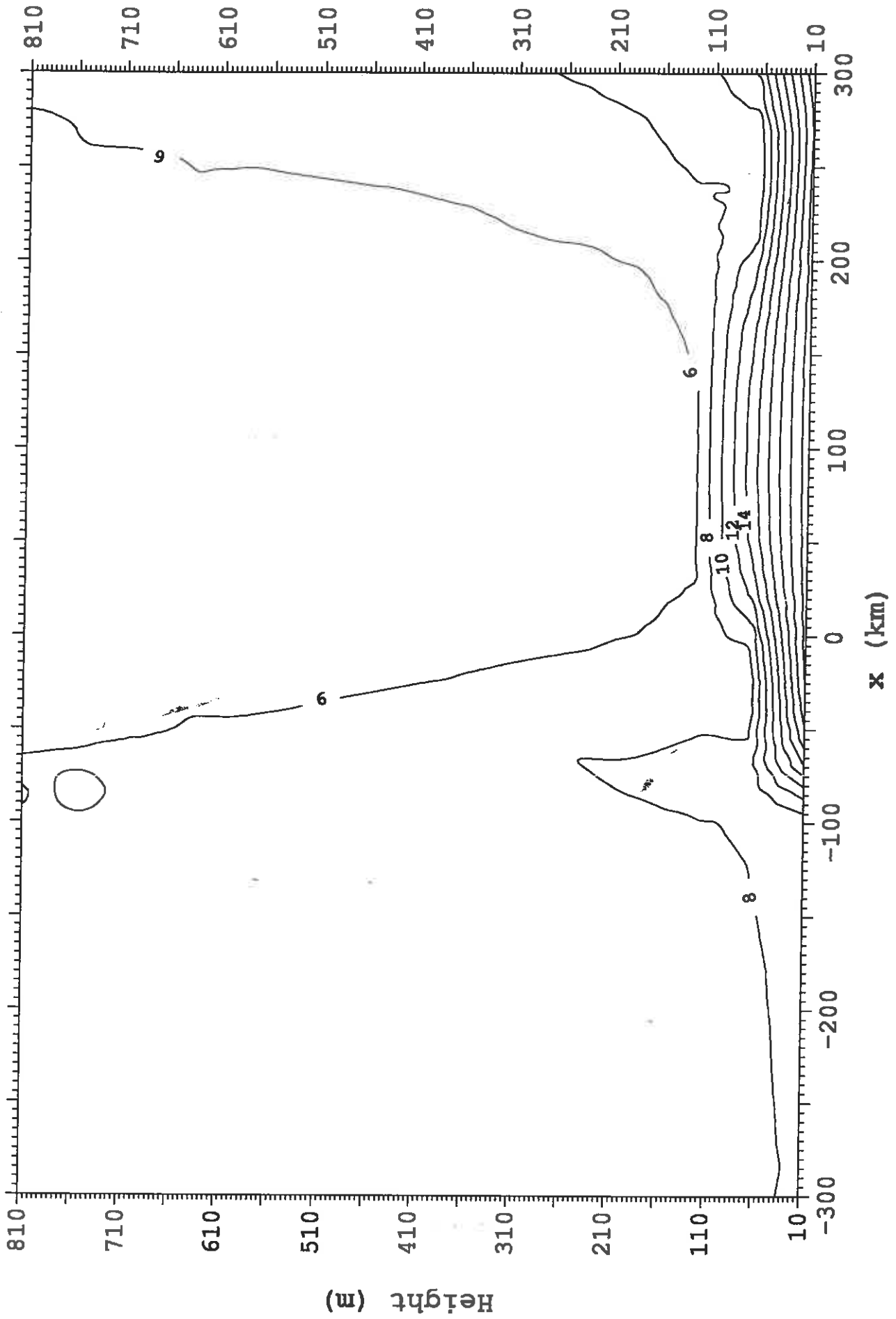
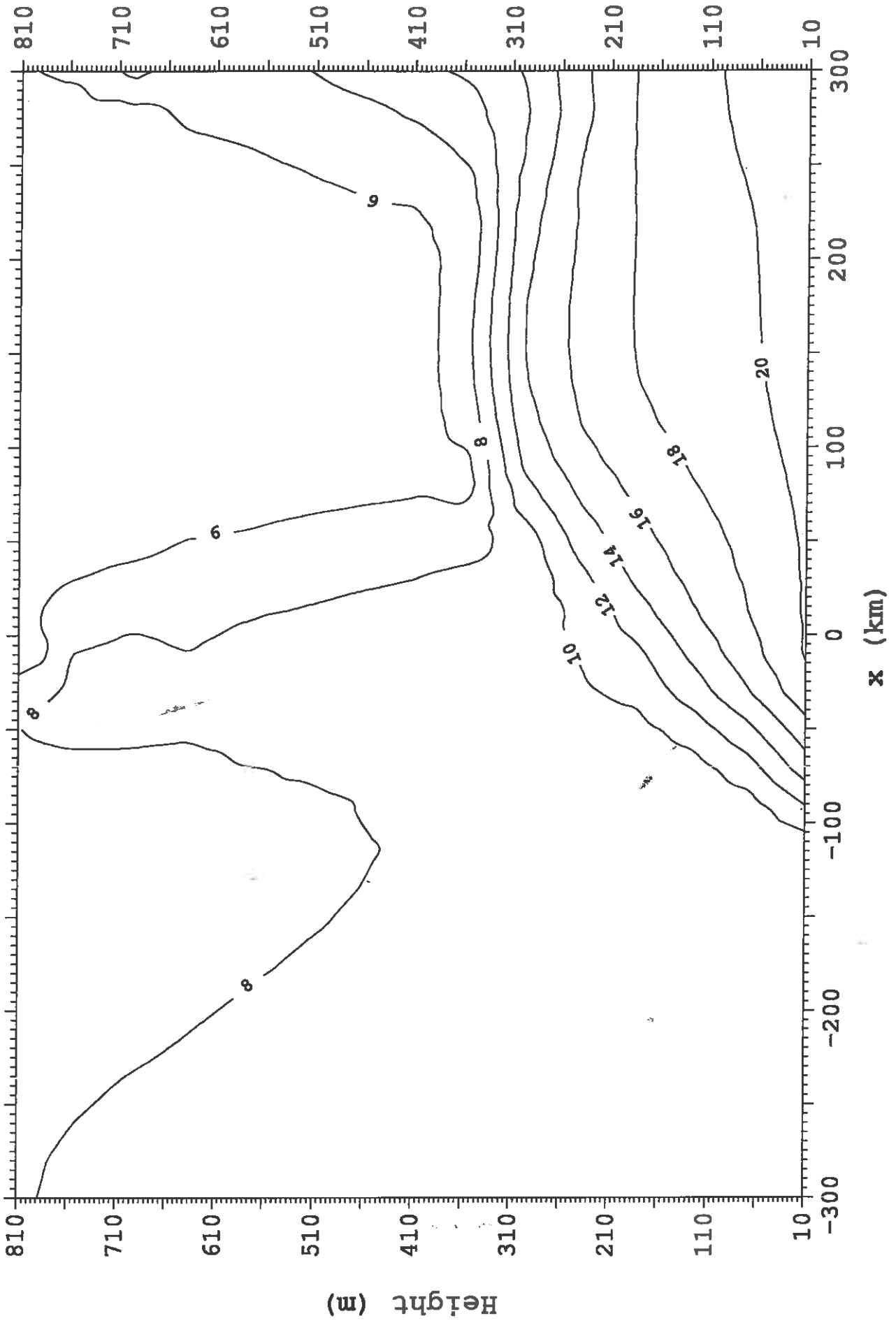Fig 3c. Vapour pressure (mb) along Y=-54km at 1400 with 9km grid length
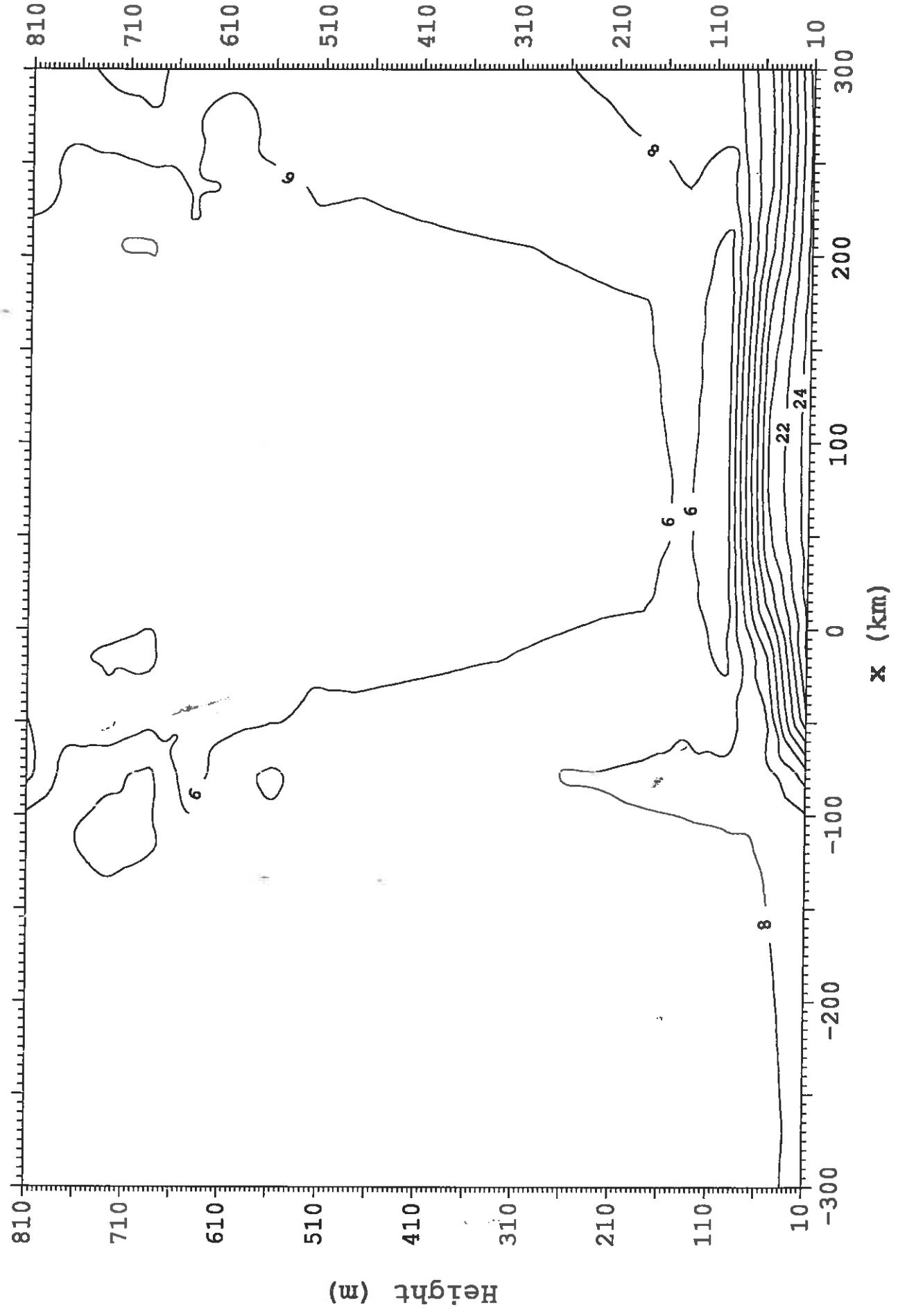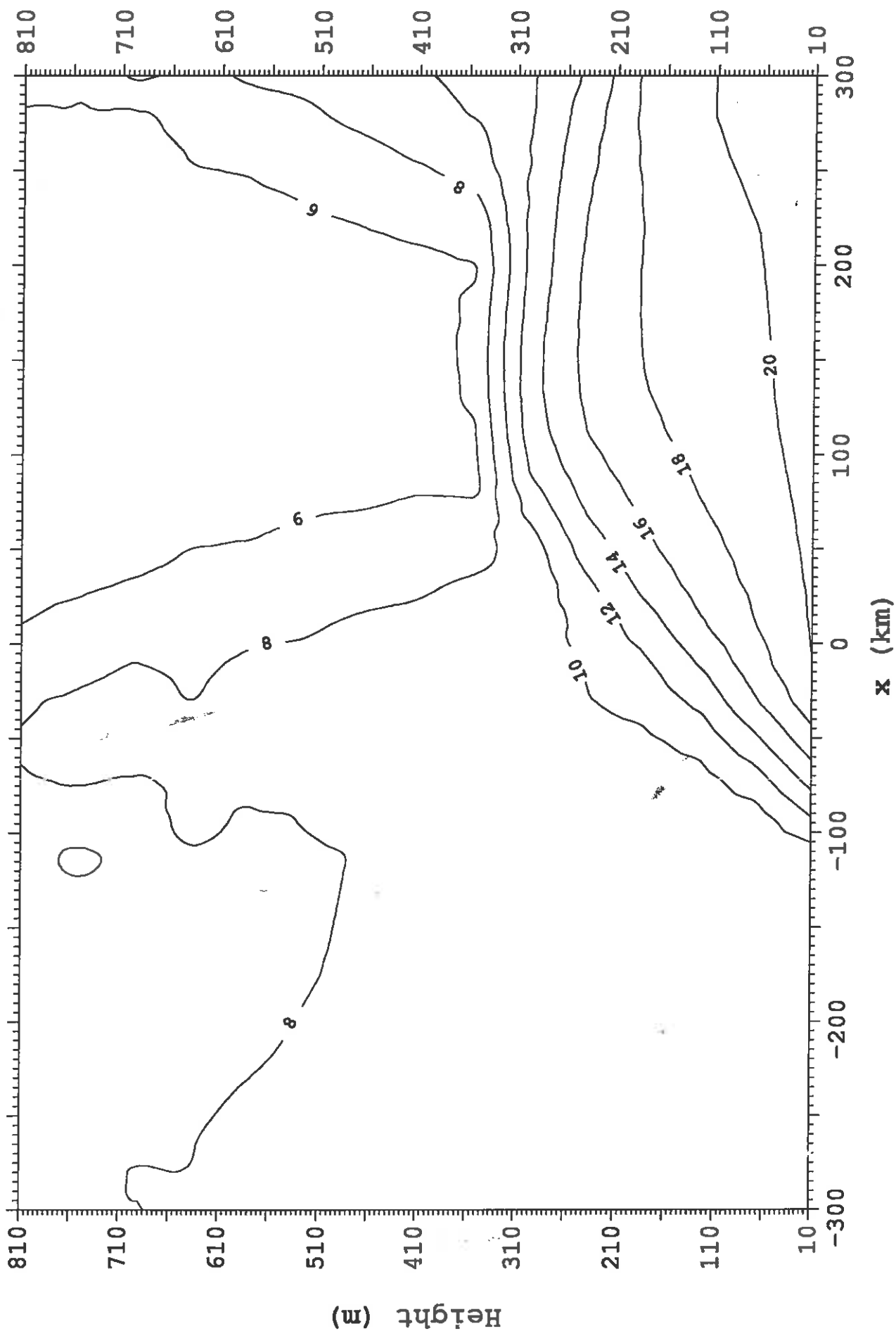
Fig 3d. Vapour pressure (mb) along Y=-54km at 1400 with 12km grid length
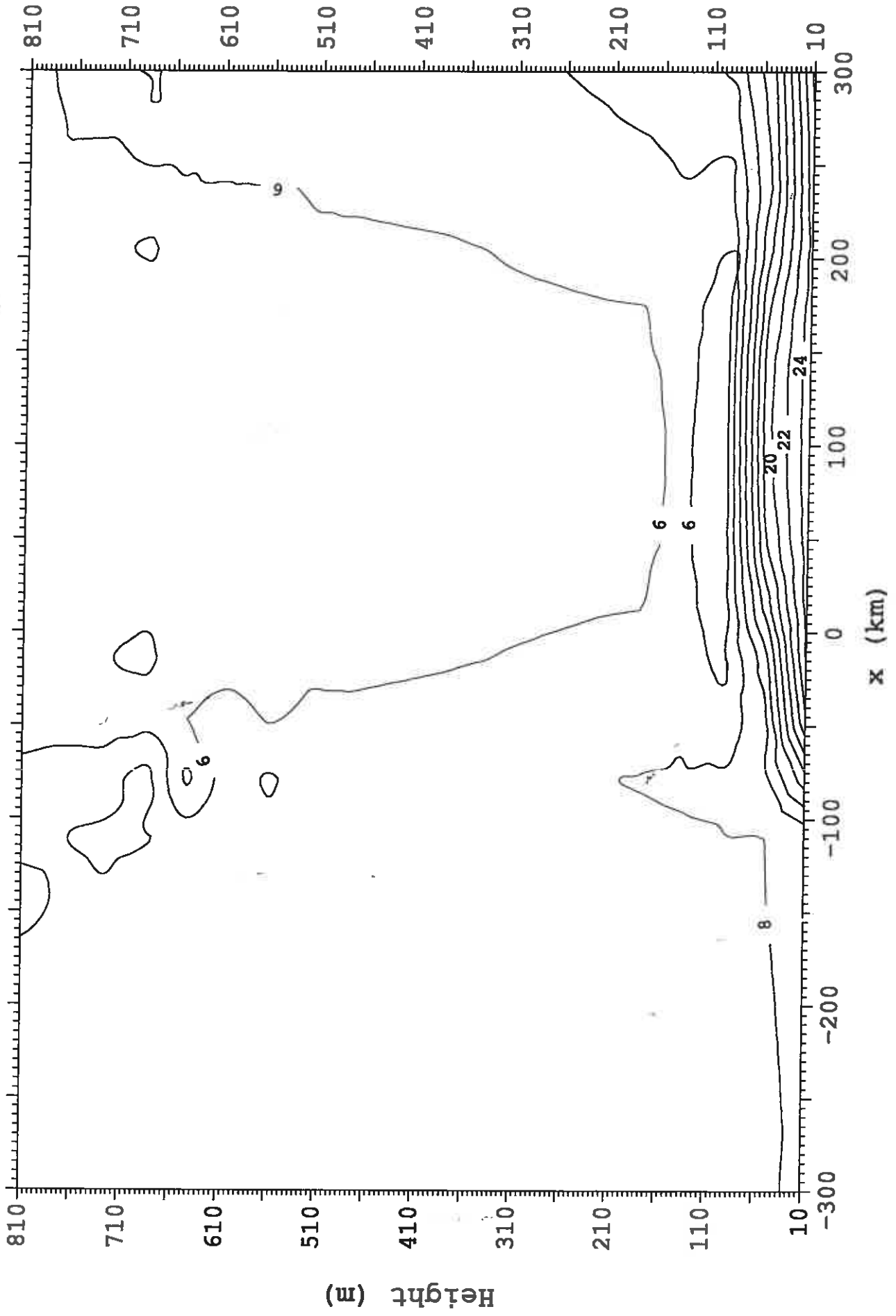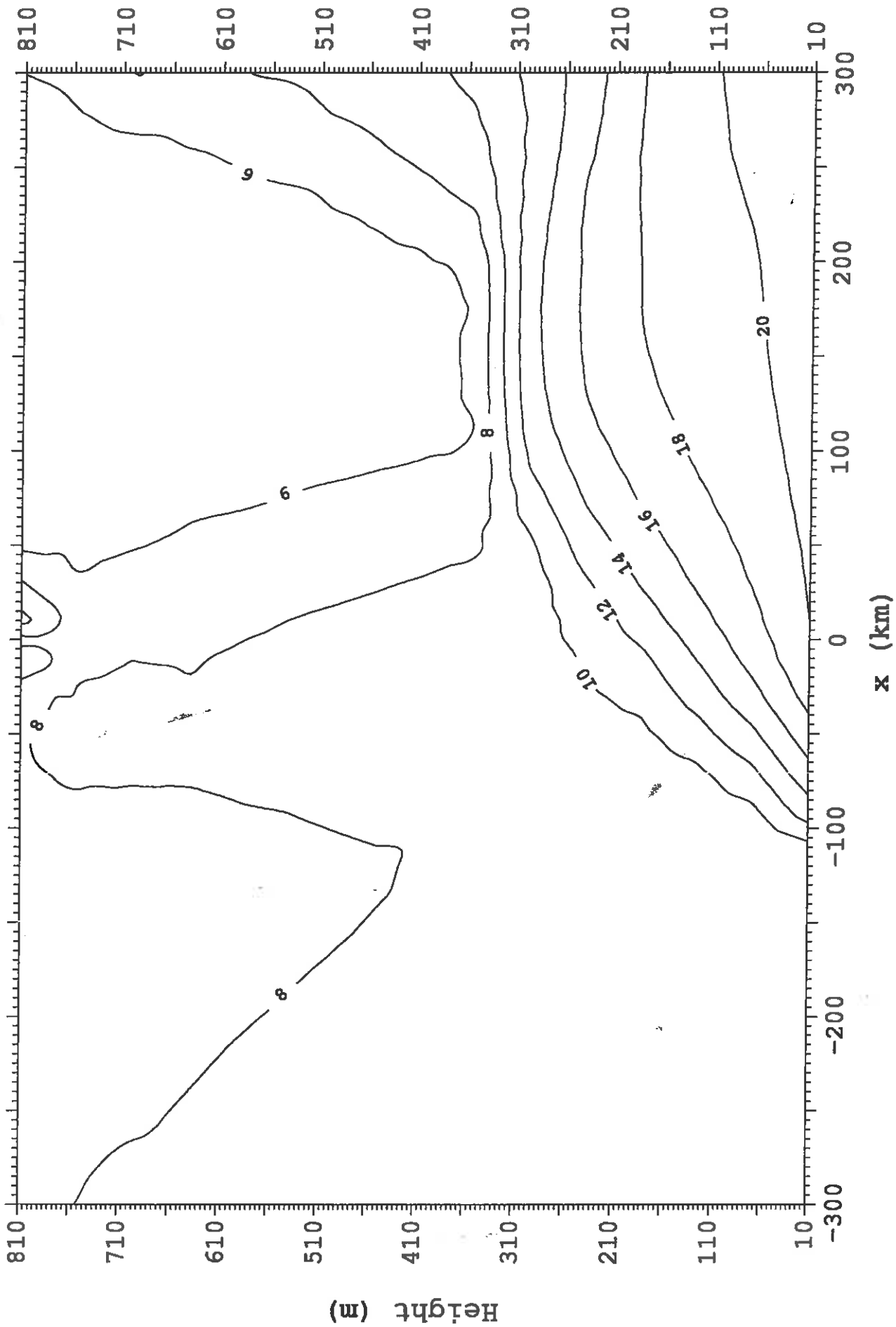
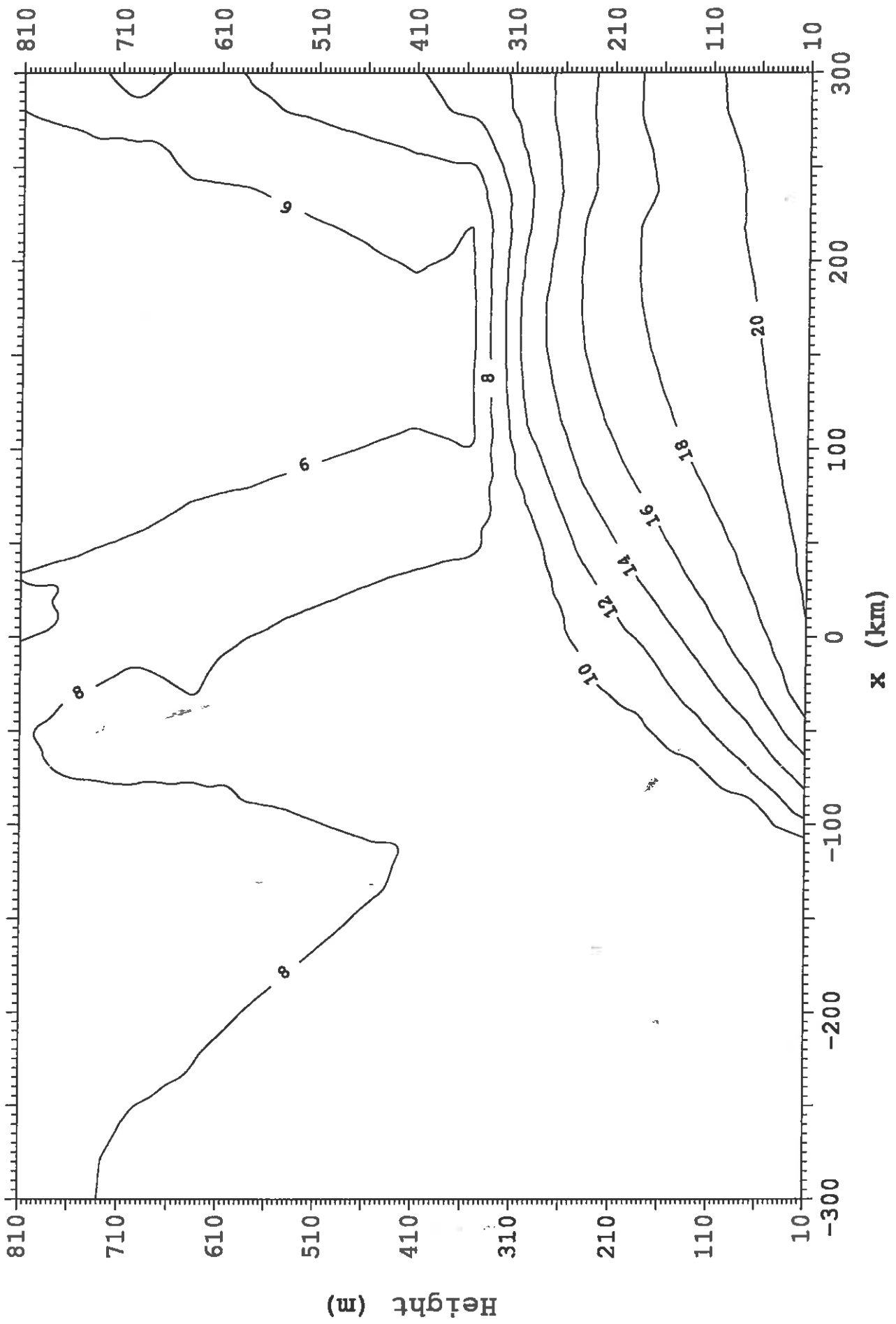Fig 3e. Vapour pressure (mb) along Y=-54km at 1400 with 15km grid length
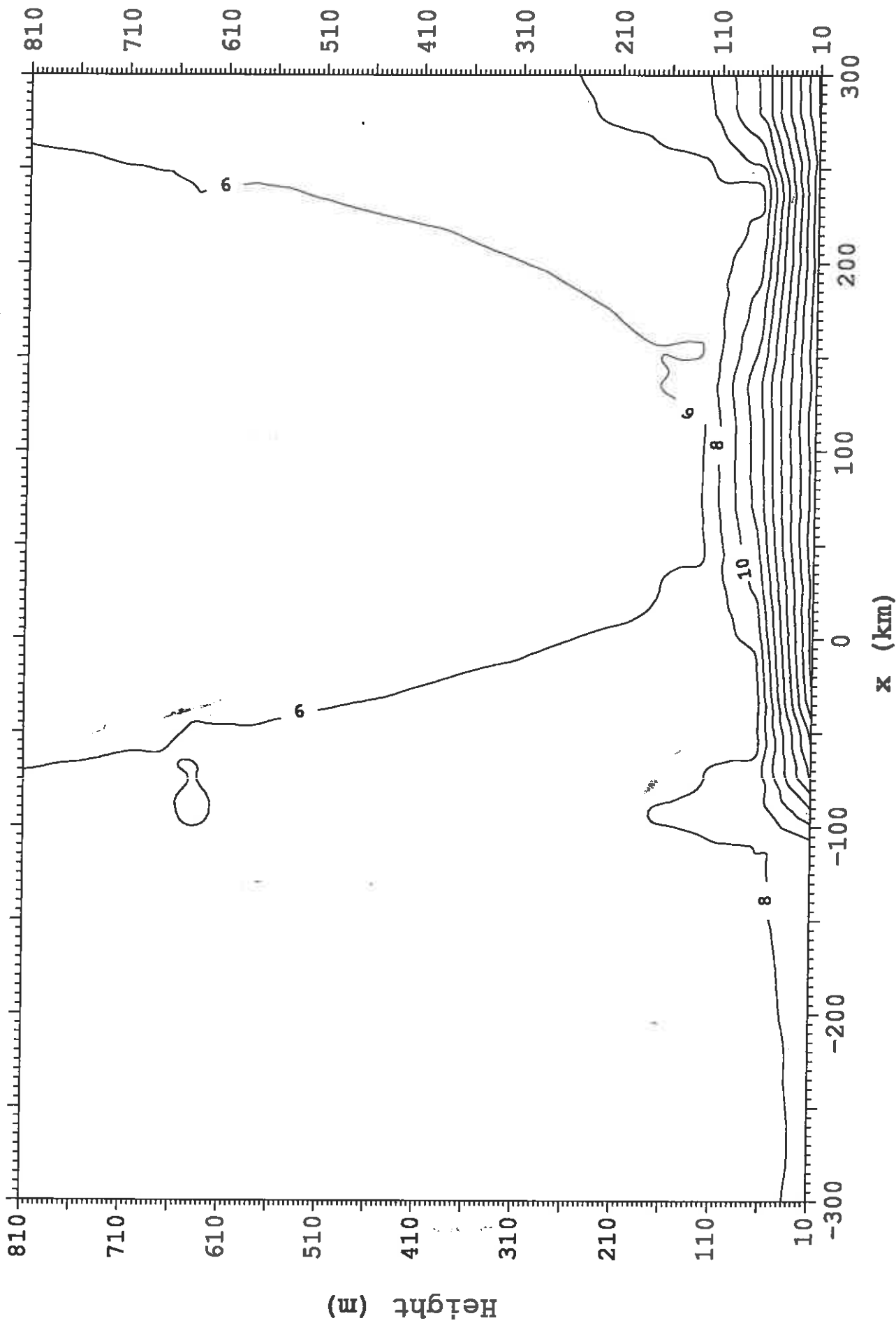
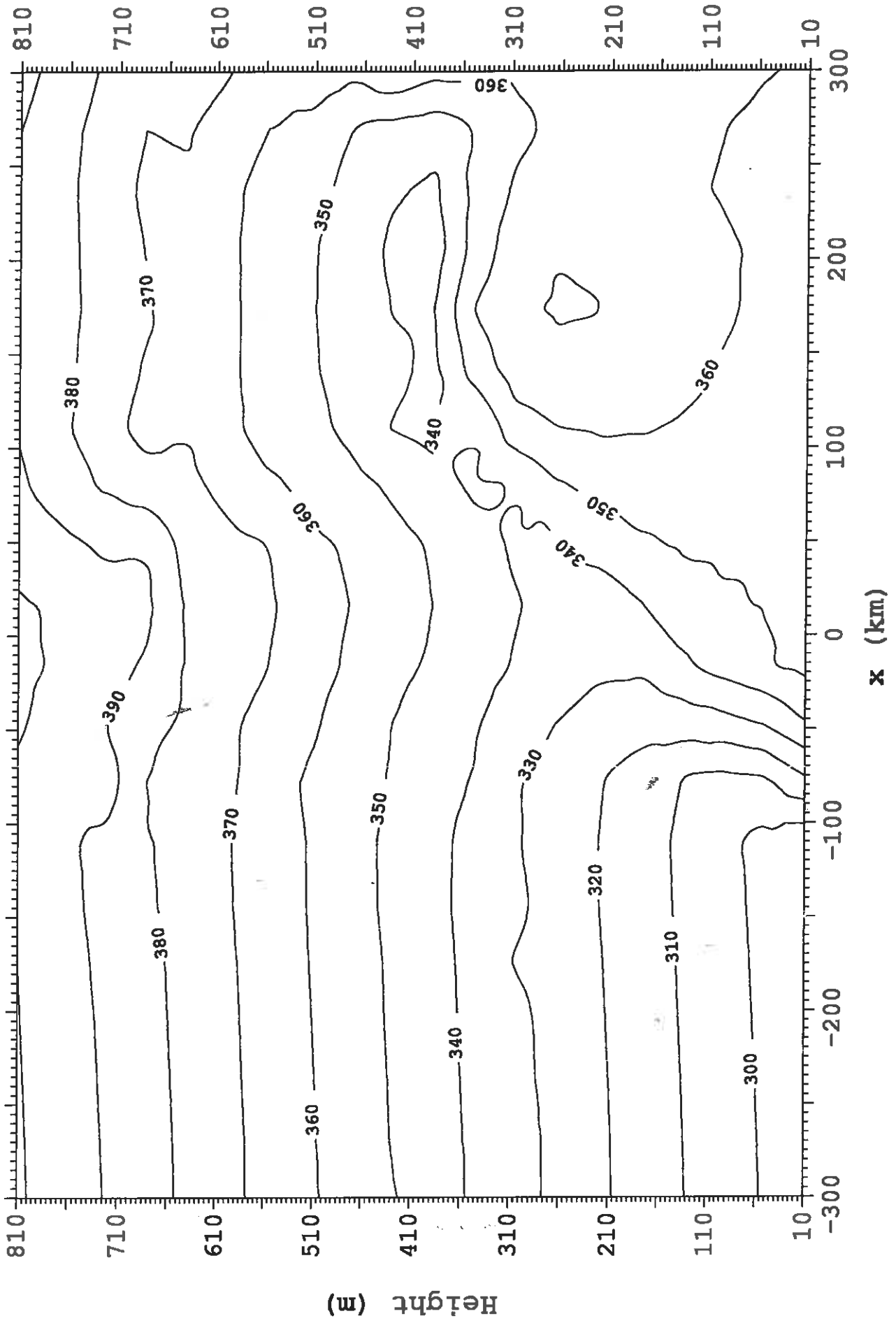Fig 4a. Refractivity along Y=-54km at 1500 with 3km grid length
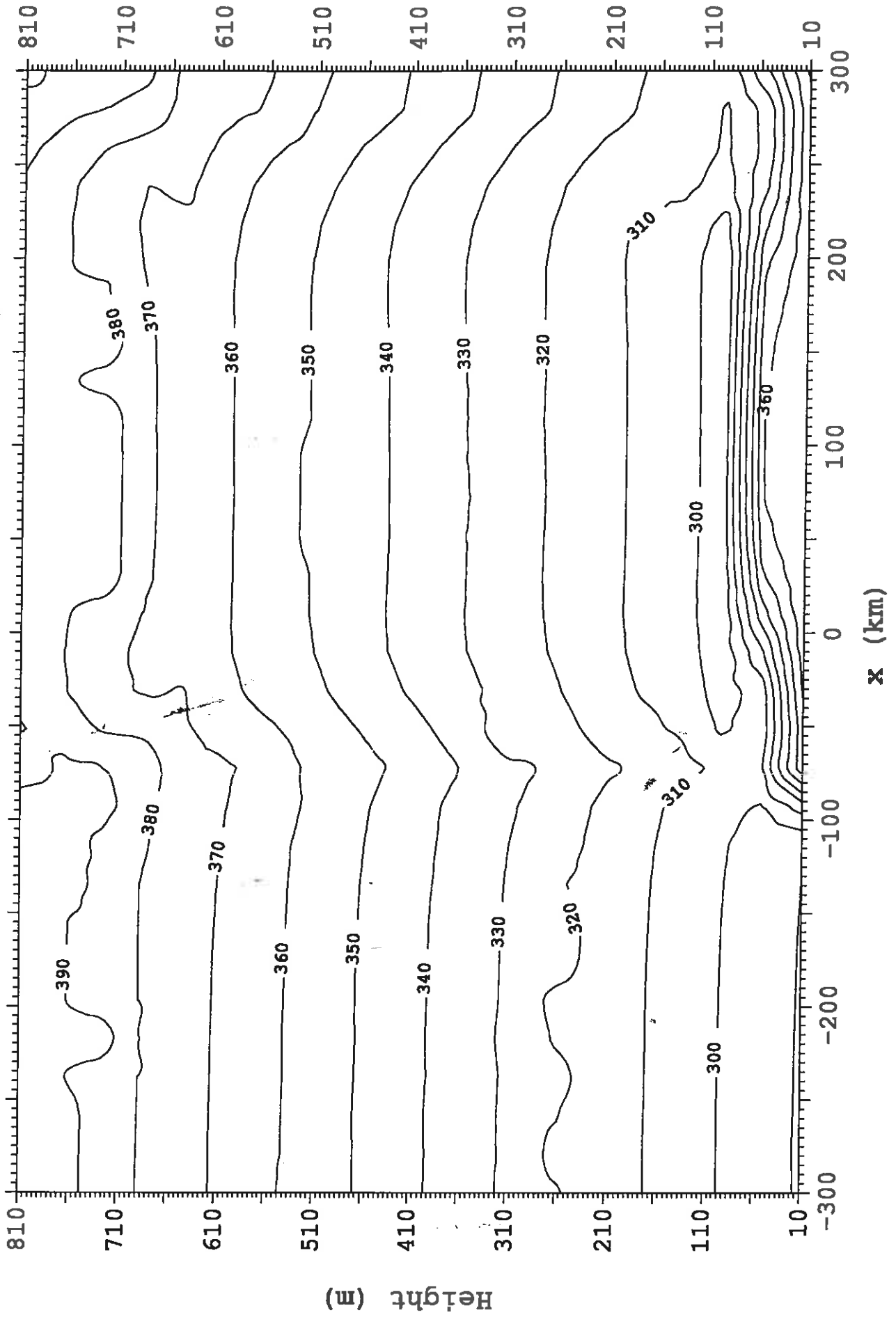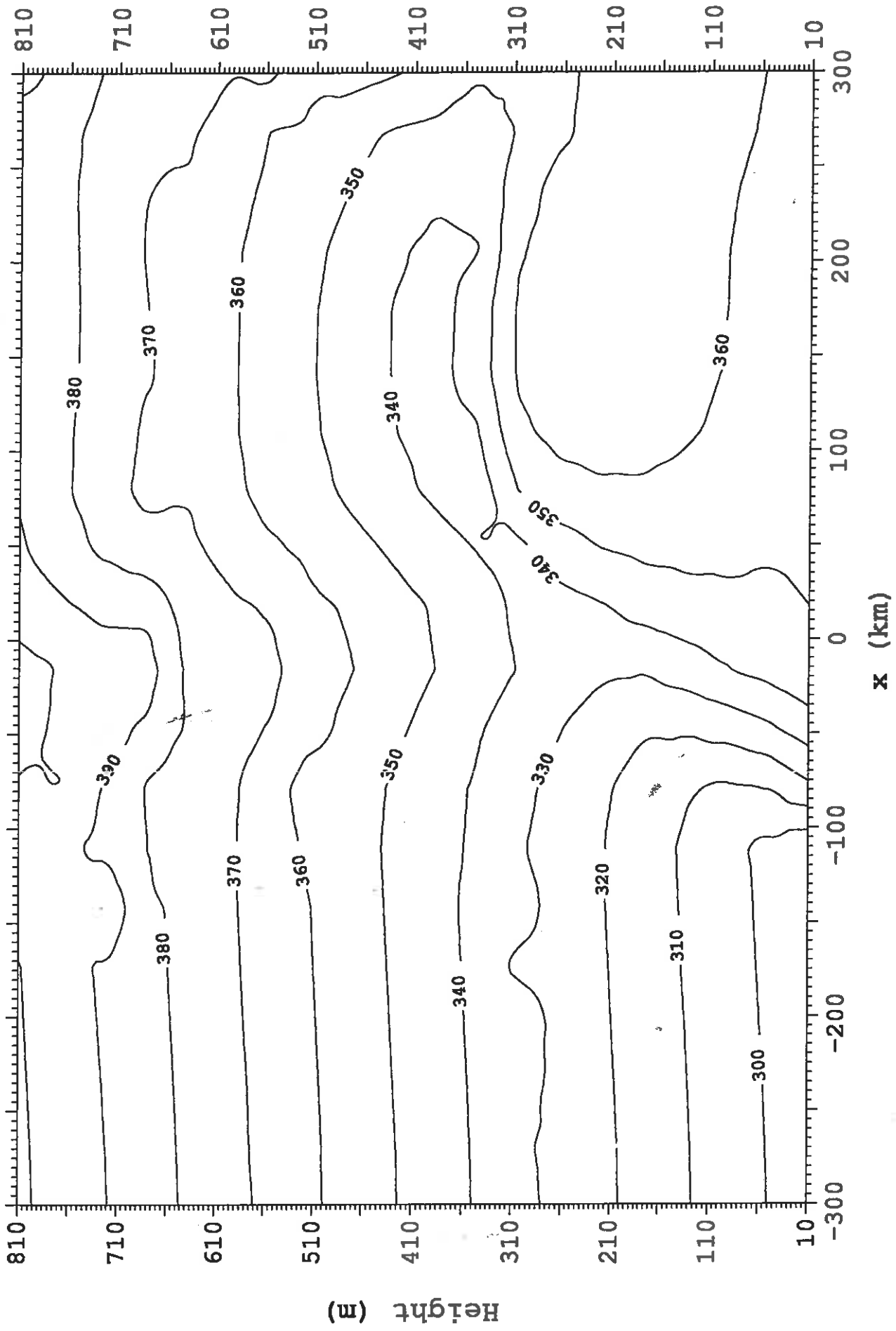
Fig 4b. Refractivity along Y=-54km at 1400 with 6km grid length
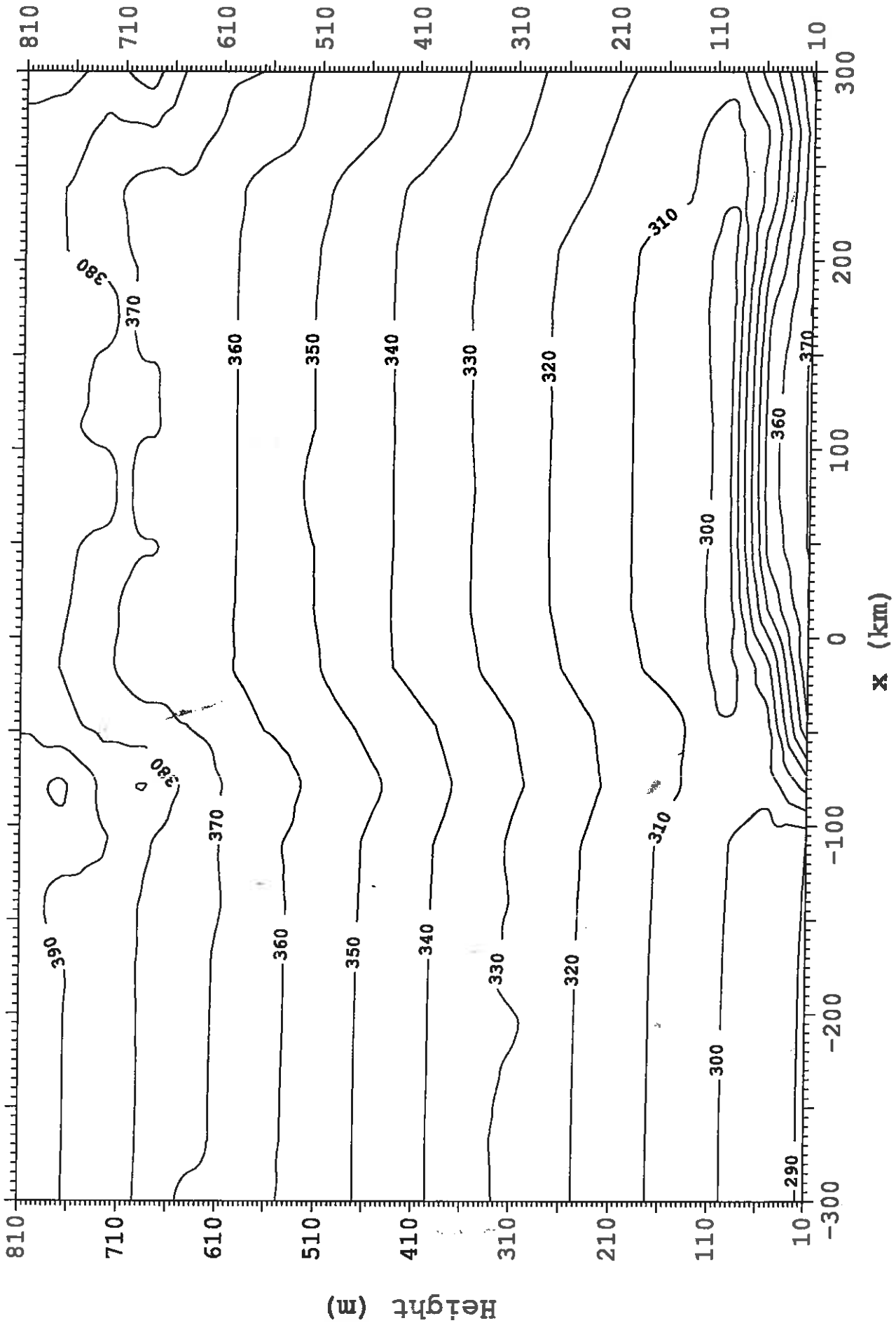
Fig 4c. Refractivity along Y=-54km at 1400 with 9km grid length
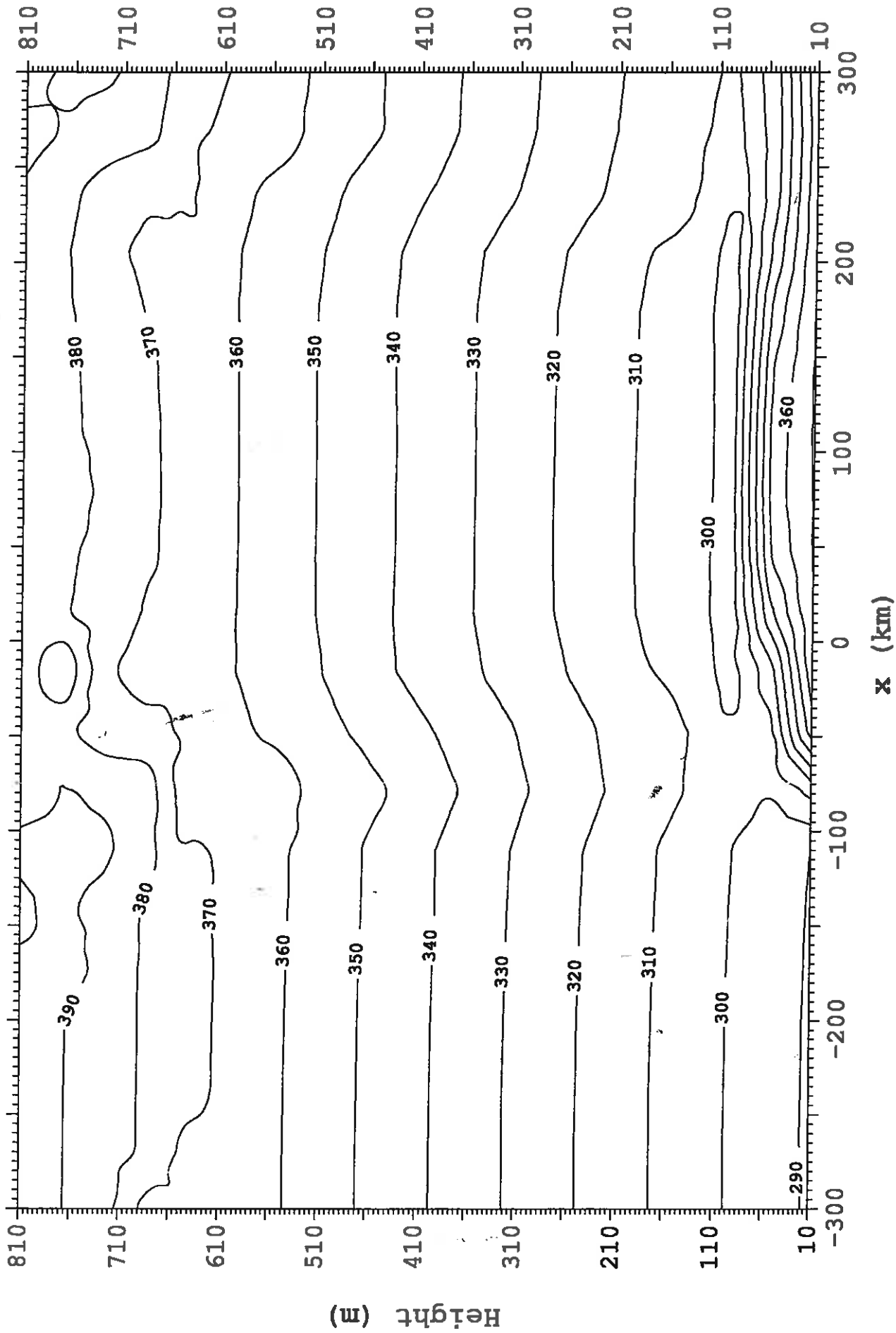
Fig 4d. Refractivity along Y=-54km at 1400 with 12km grid length
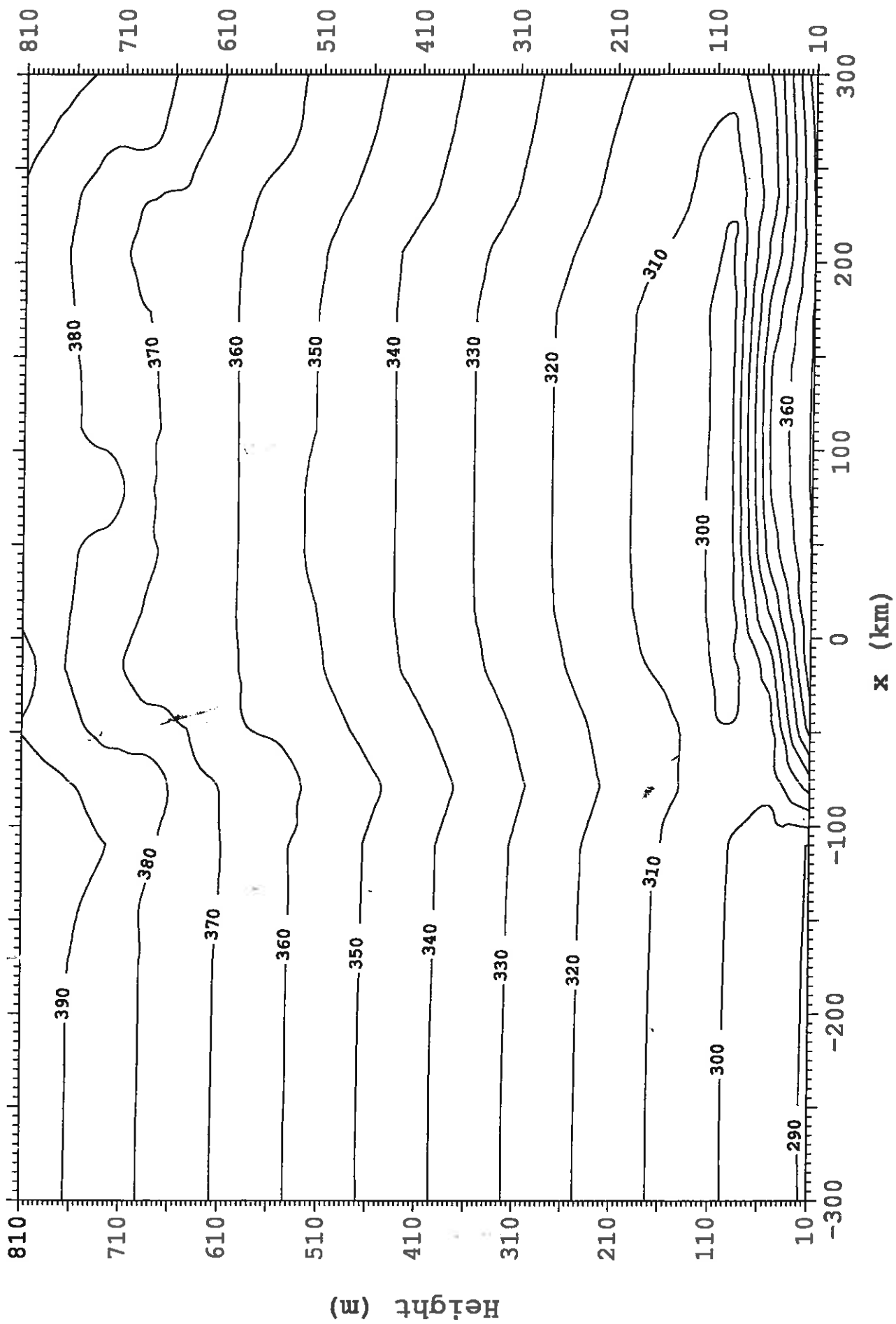
Fig 4e. Refractivity along Y=-54km at 1400 with 15km grid length
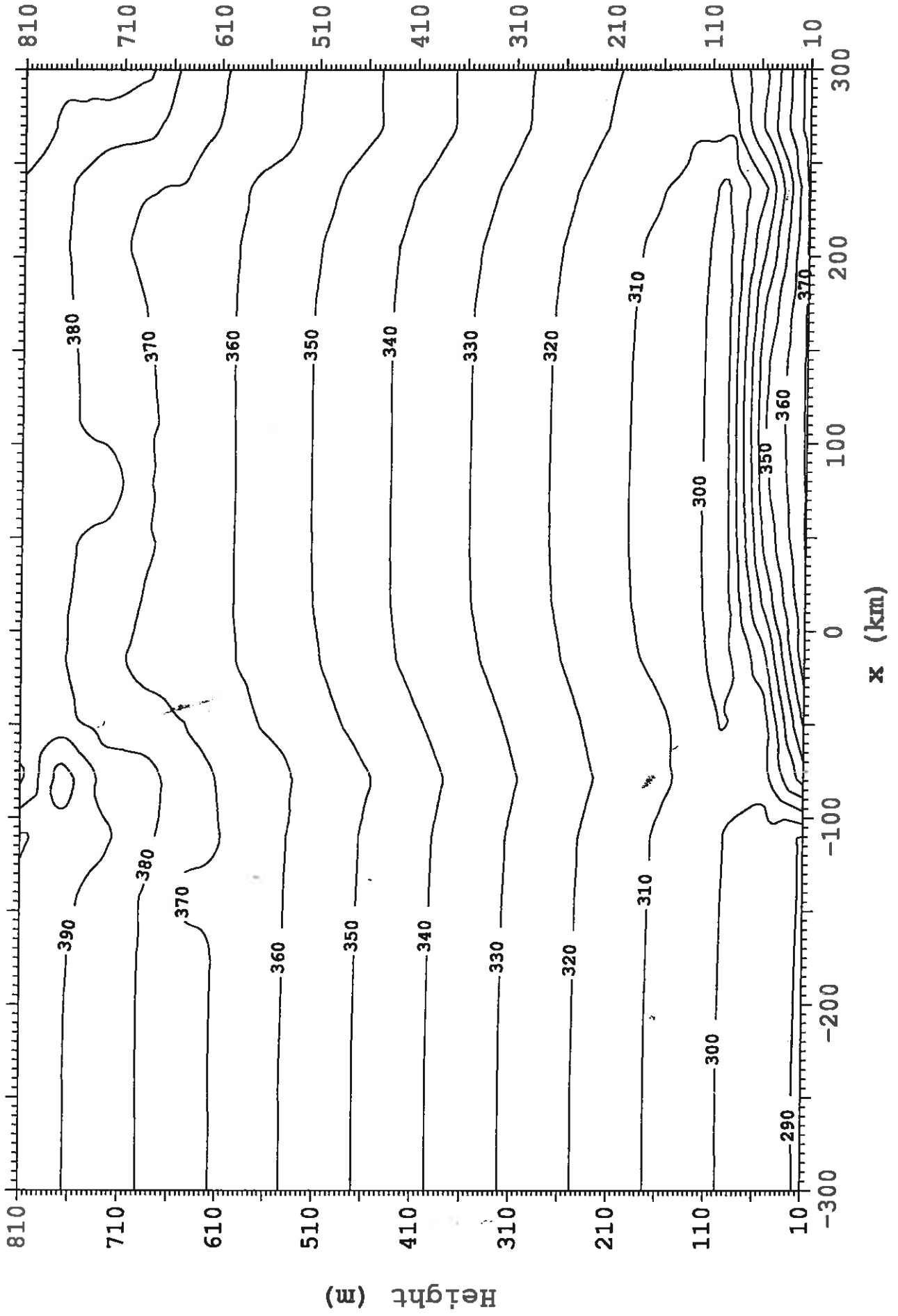
Fig 5a. Winds U (m/s) and W (cm/s) along Y=-54km at 1500 with 3km grid length
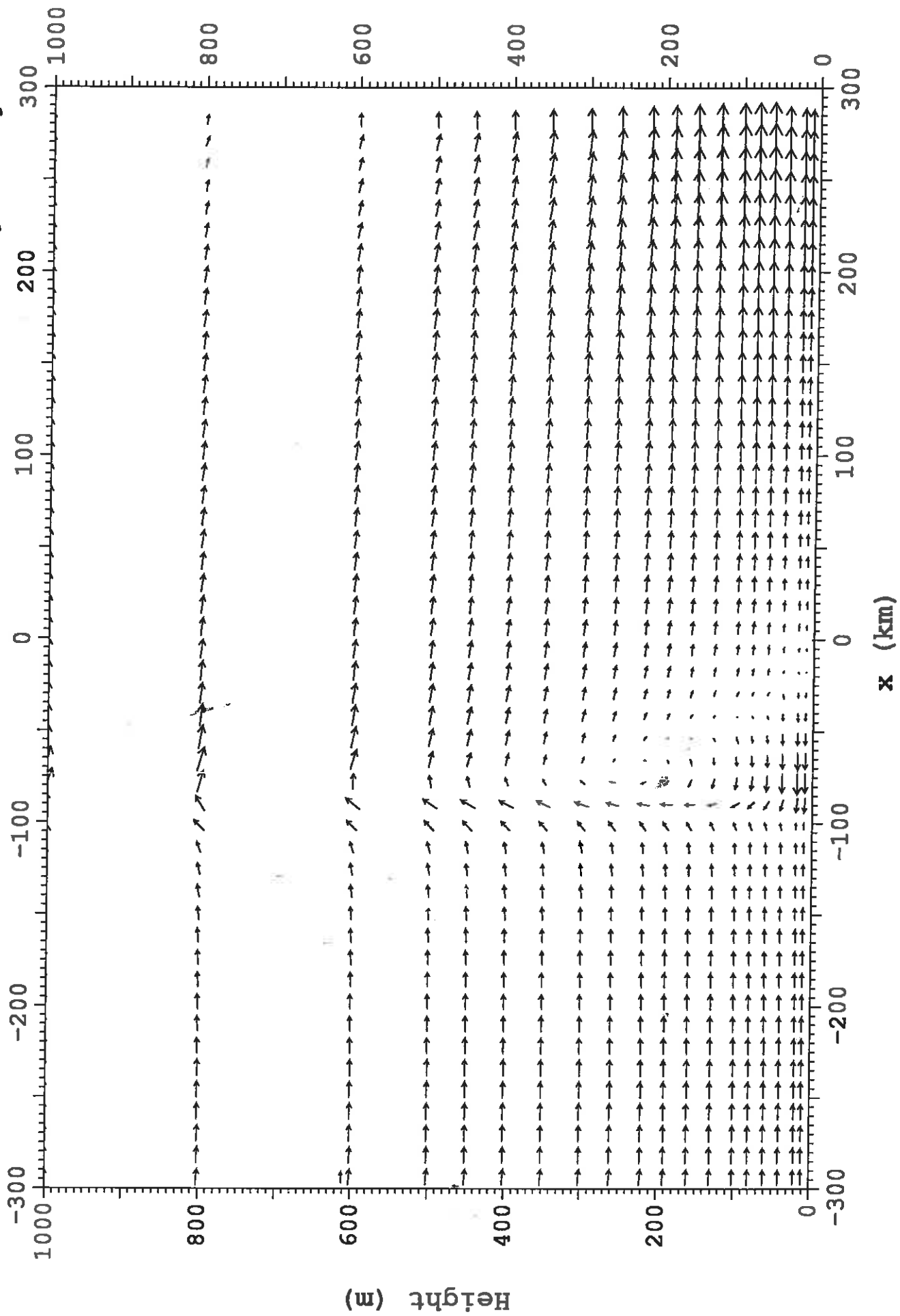
Fig 5b. Winds U (m/s) and W (cm/s) along Y=-54km at 1400 with 6km grid length
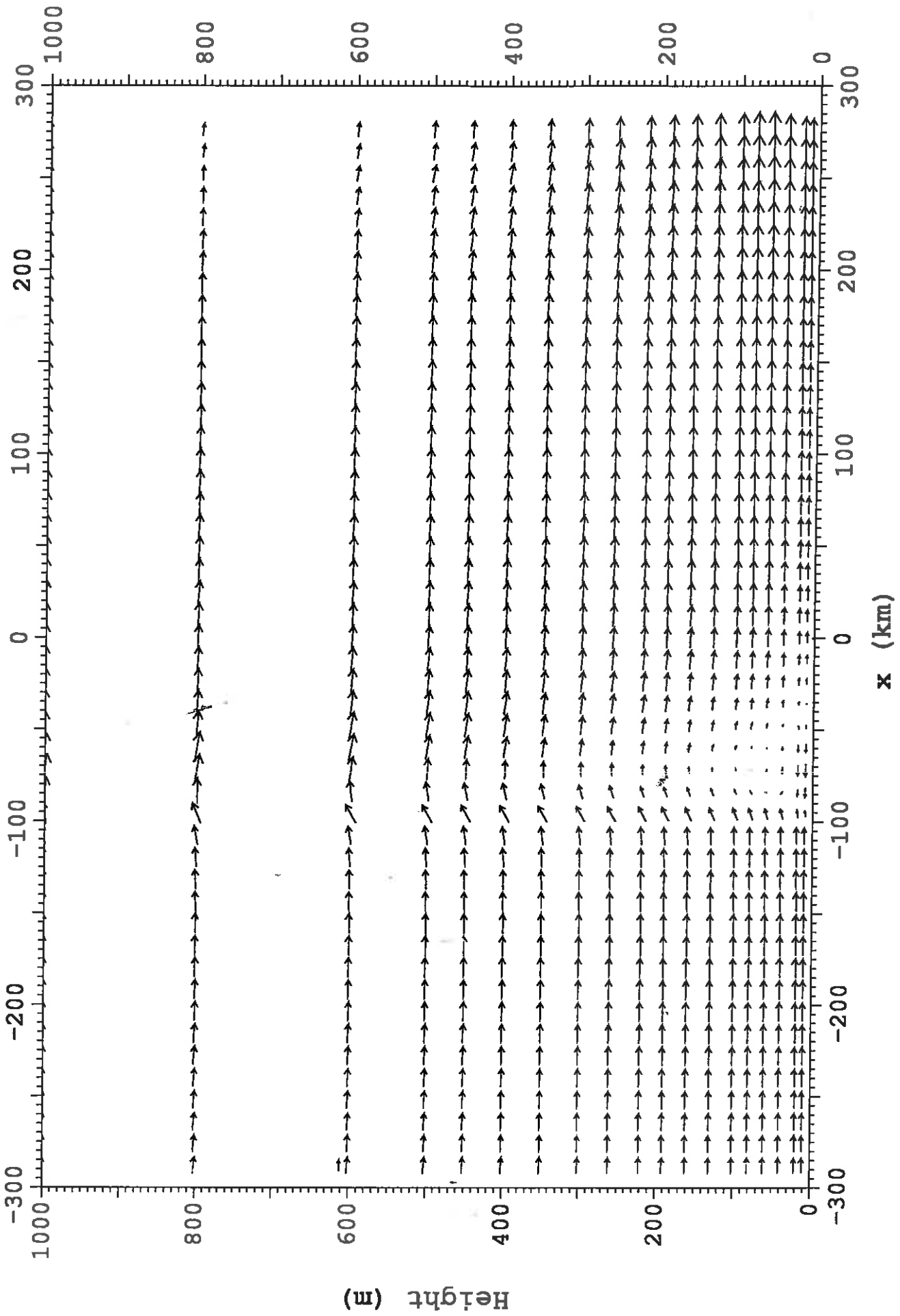
Fig 5c. Winds U (m/s) and W (cm/s) along Y=-54km at 1400 with 9km grid length
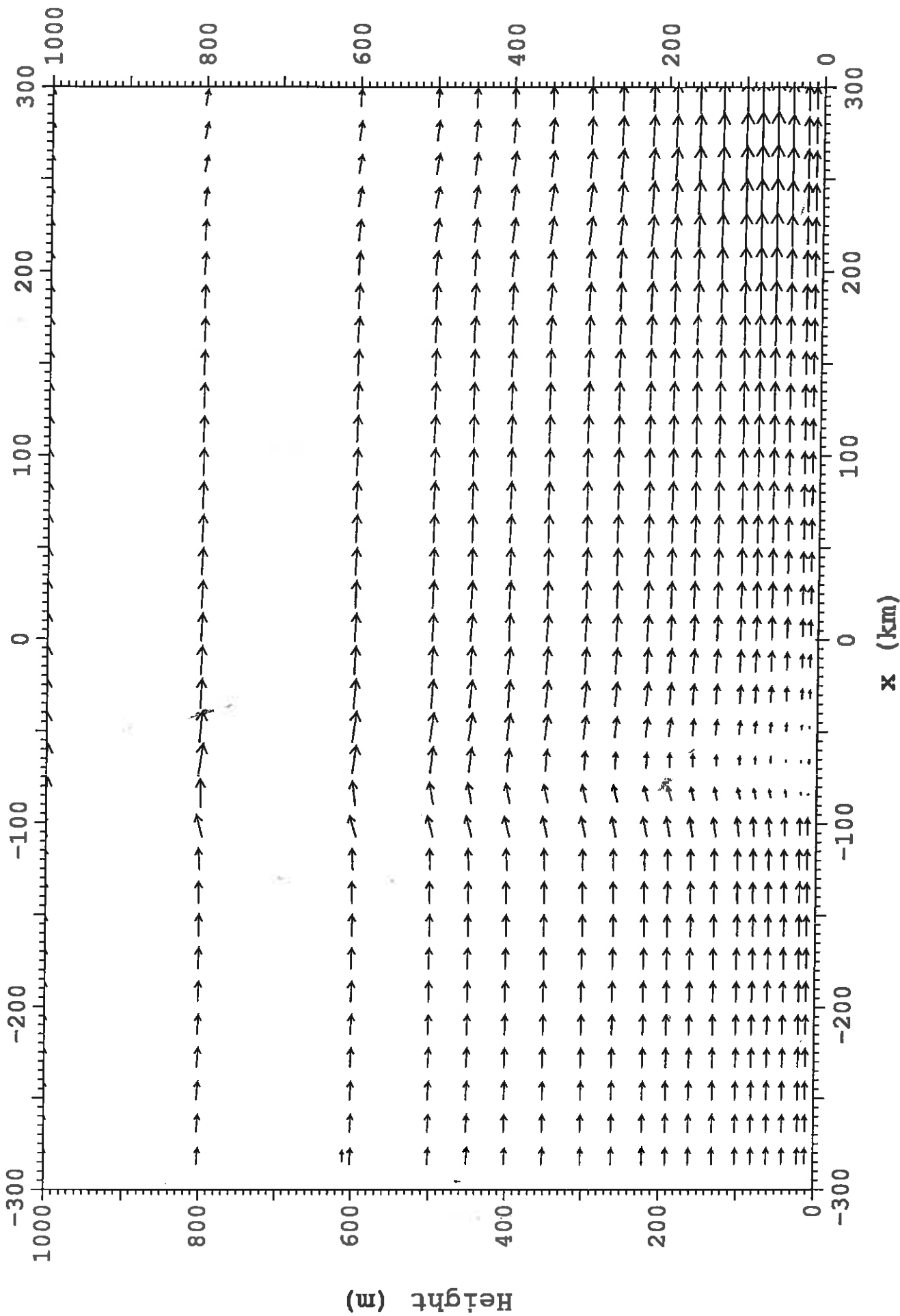
Fig 5d. Winds U (m/s) and W (cm/s) along Y=-54km at 1400 with 12km grid length
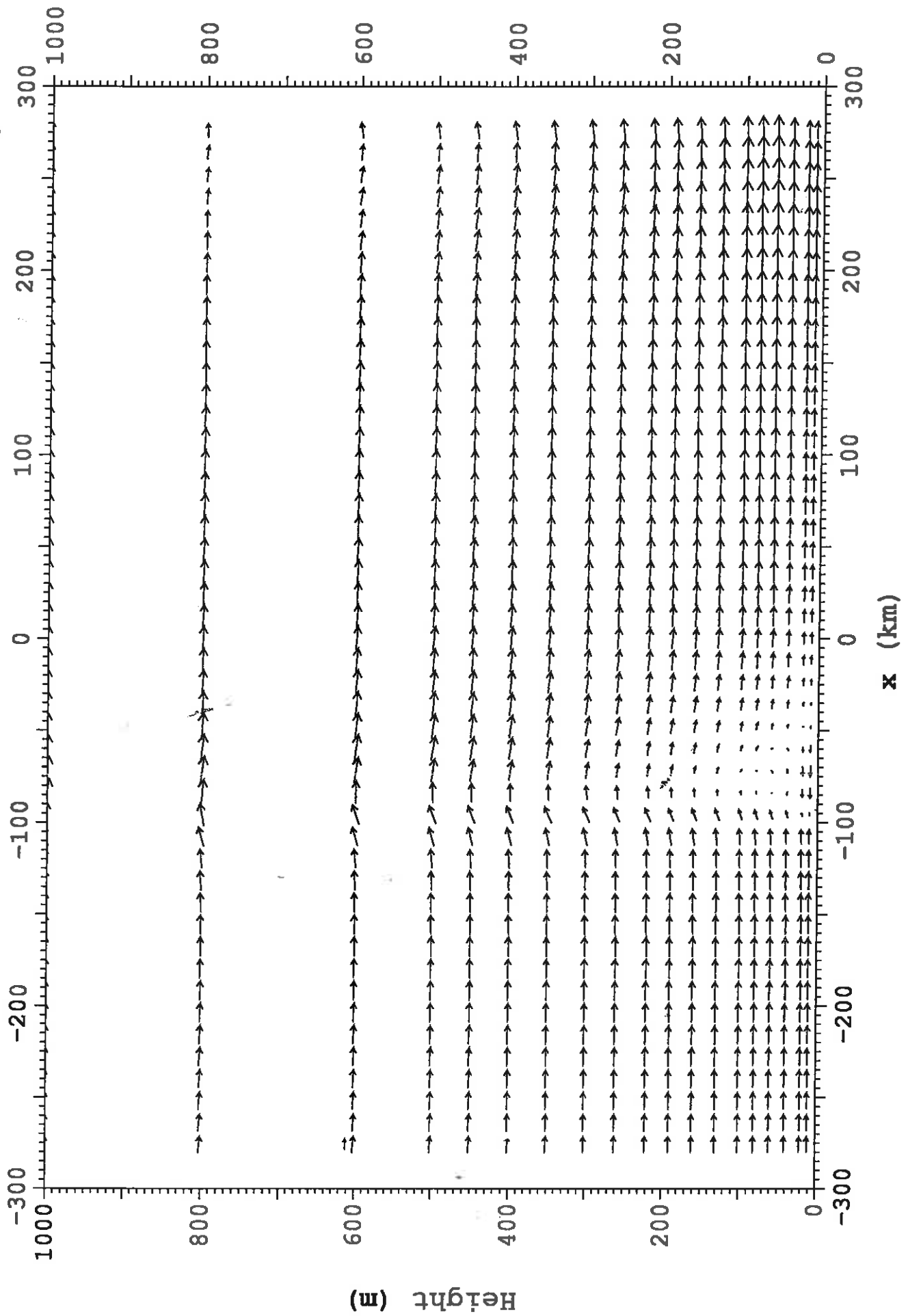
Fig 5e. Winds U (m/s) and W (cm/s) along Y=-54km at 1400 with 15km grid length
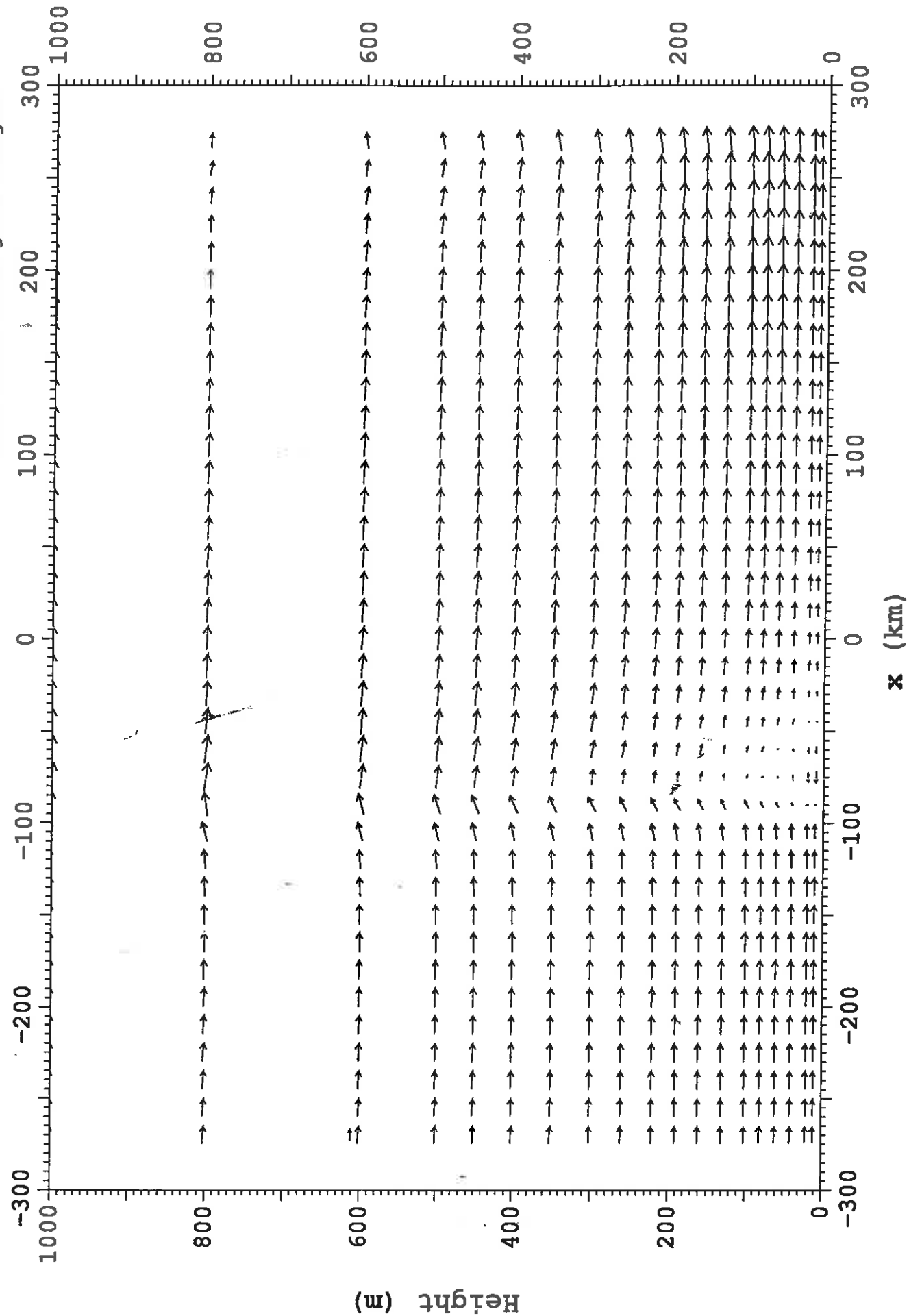
Fig 5e. Winds U (m/s) and W (cm/s) along Y=-54km at 1400 with 15km grid length
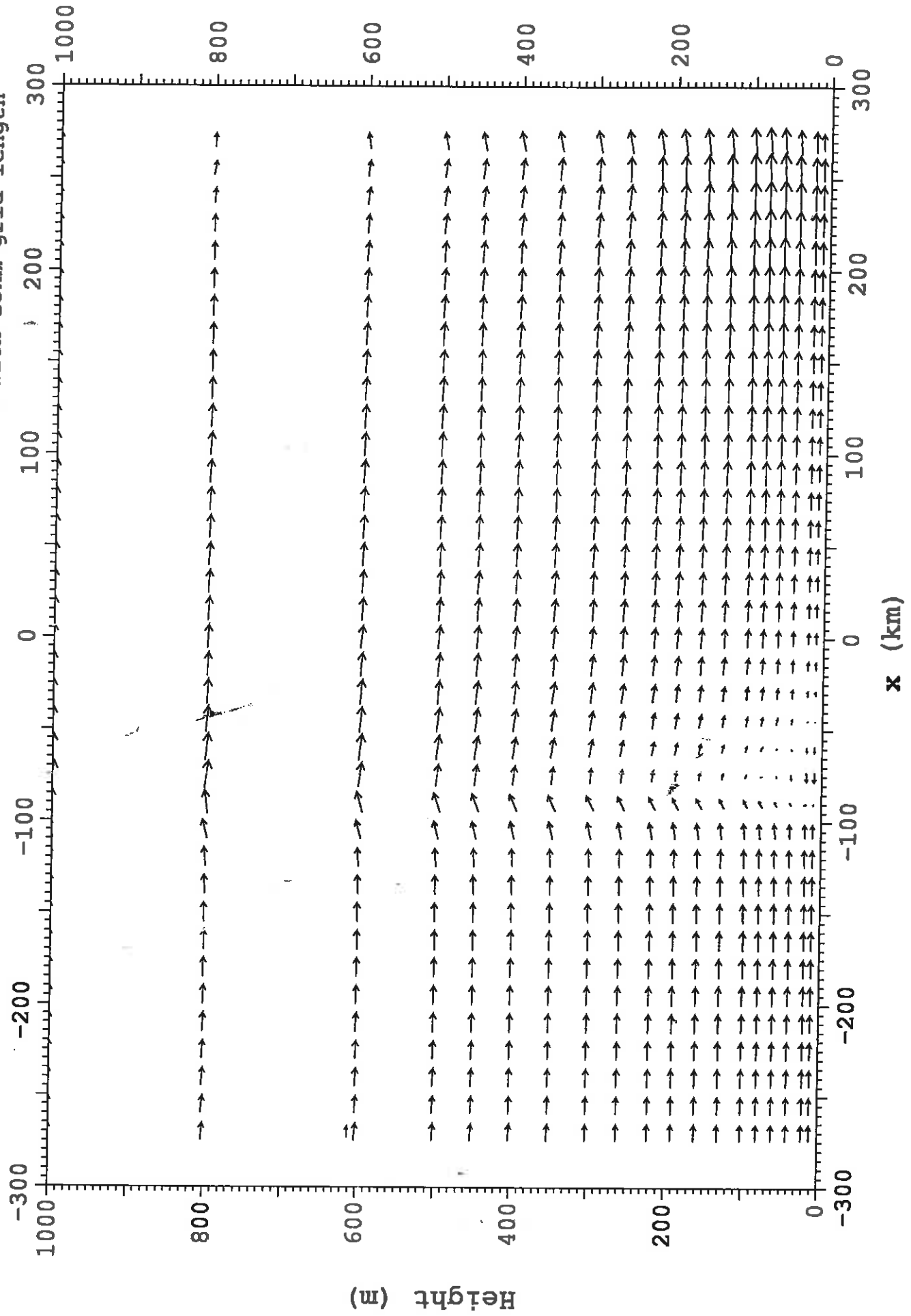
Fig 6a. Temperatures (C) along Y=-54km at 1500 with 3km grid length
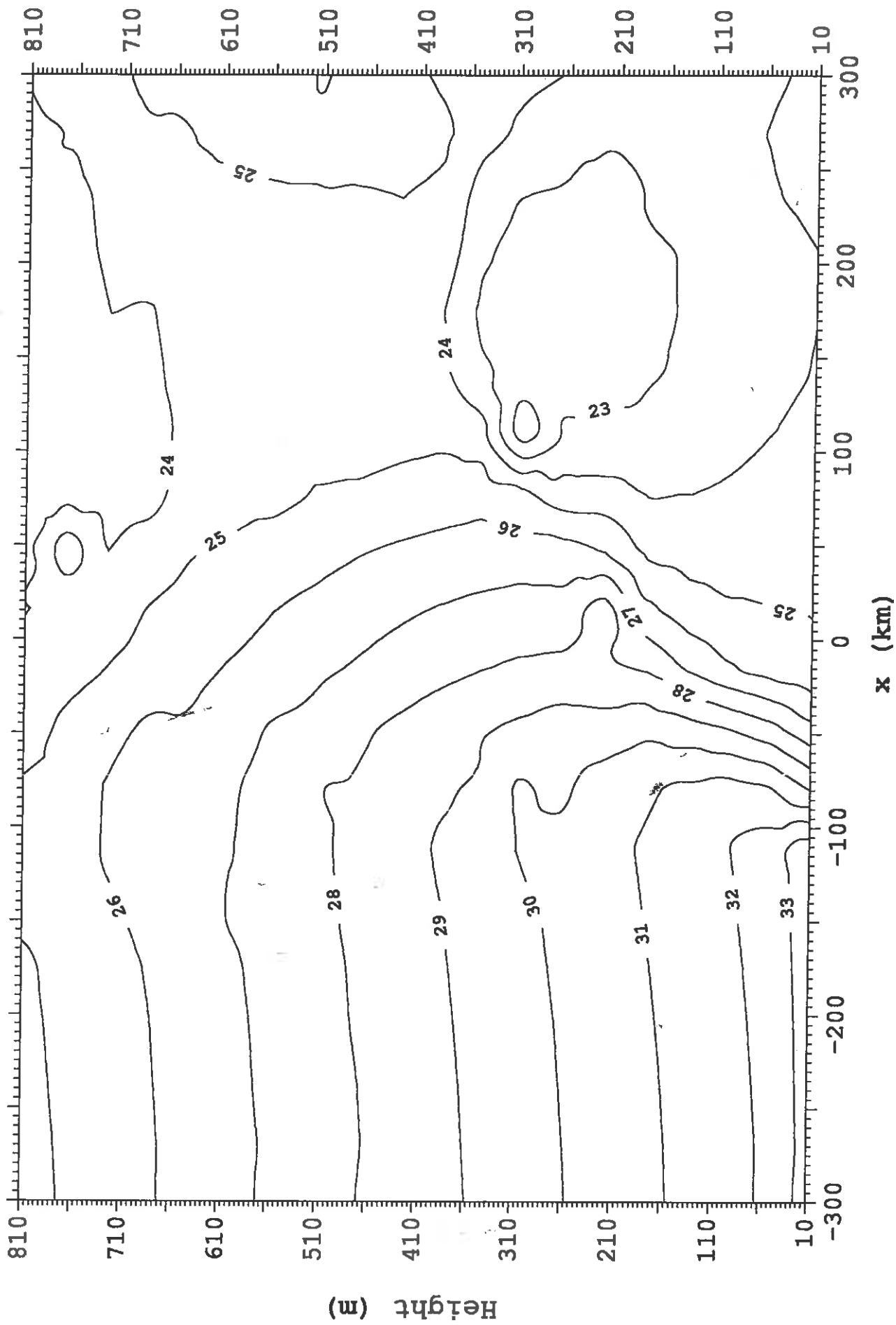
Fig 6b. Temperatures (C) along Y=-54km at 1400 with 6km grid length
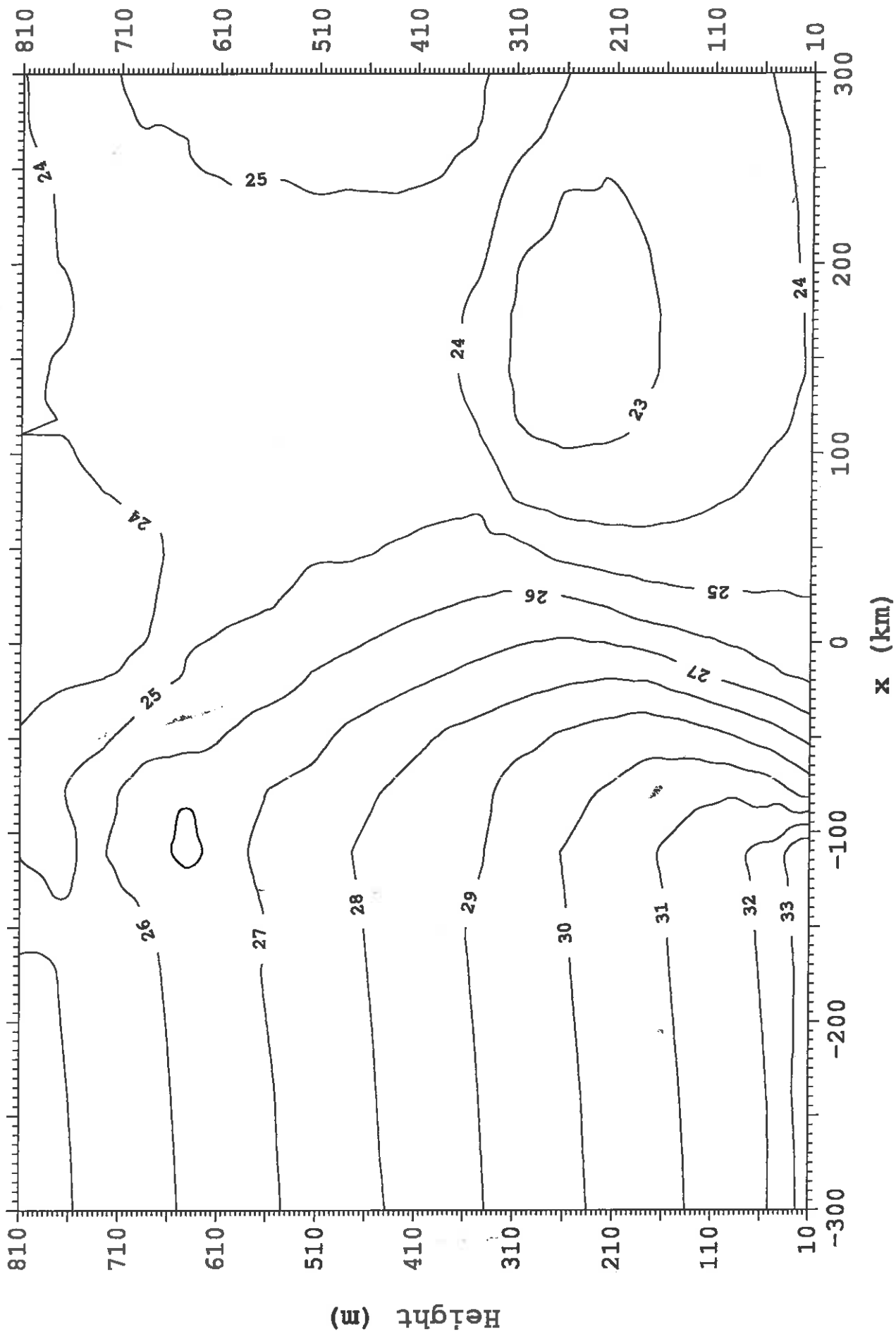
Fig 6c. Temperatures (C) along Y=-54km at 1400 with 9km grid length
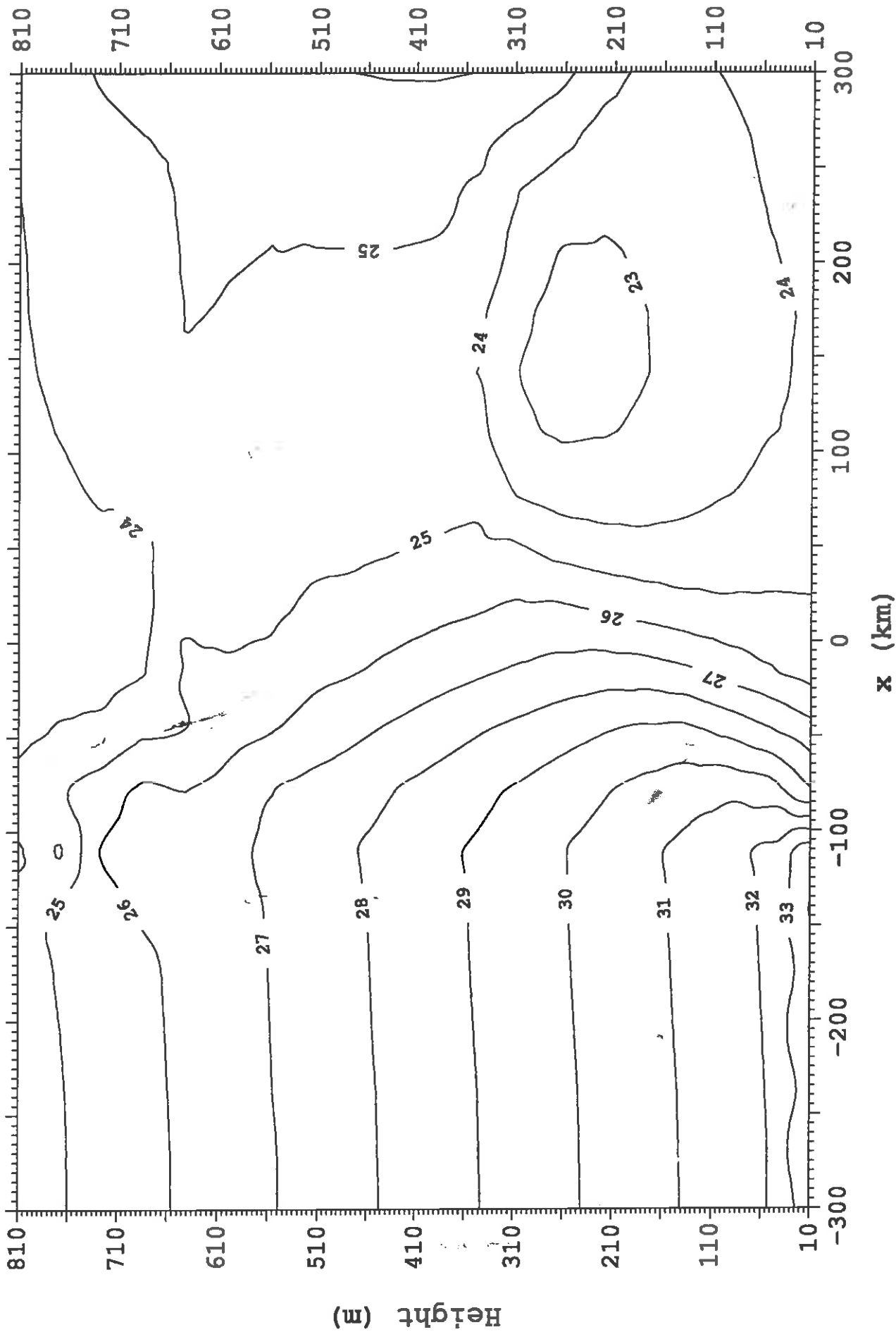
Fig 6d. Temperatures (C) along Y=-54km at 1400 with 12km grid length

Fig 6e. Temperatures (C) along Y=-54km at 1400 using 15km grid length

Fig 7a. Vapour pressure (mb) along Y=-54km at 1500 with 3km grid length
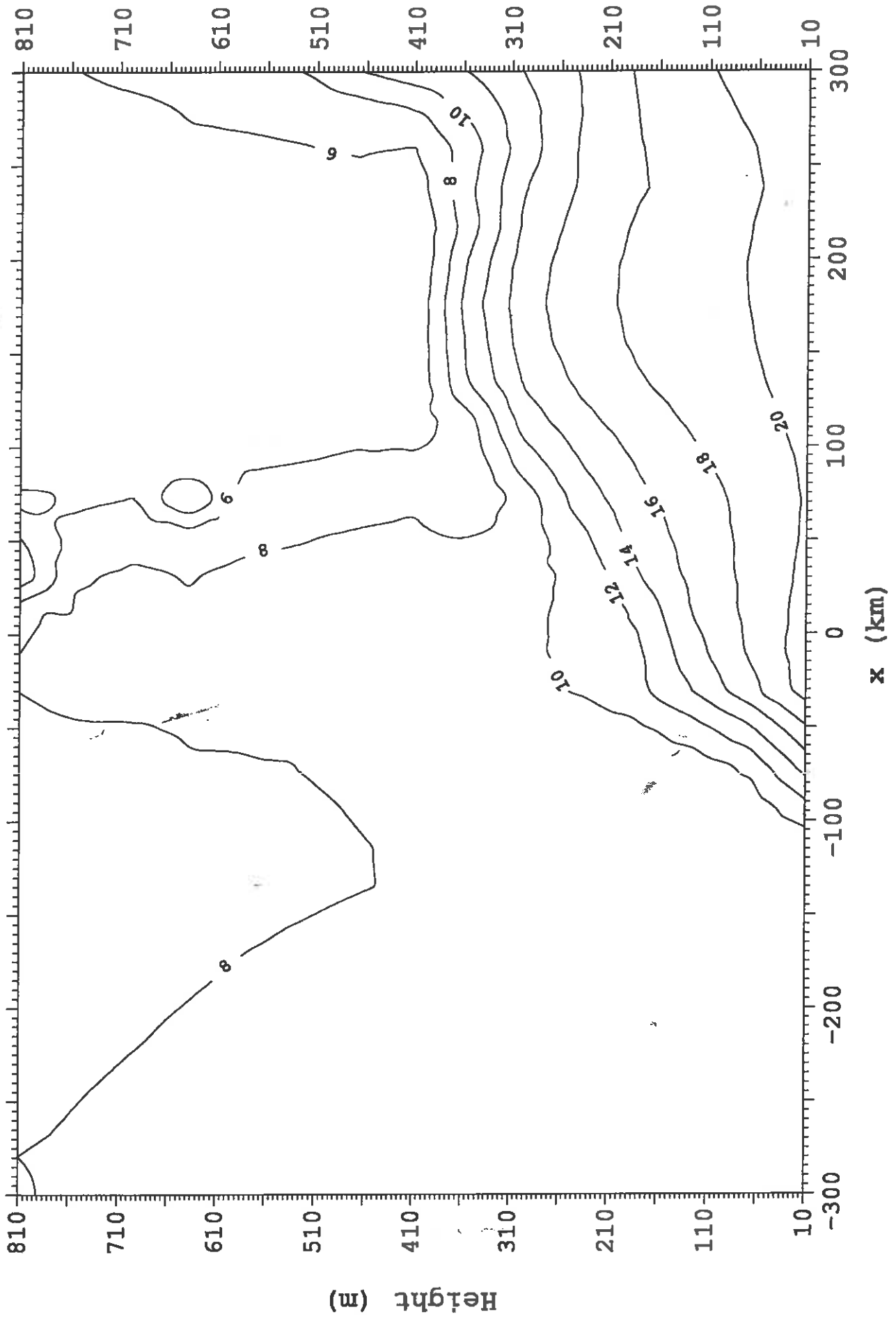
Fig 7b. Vapour pressure (mb) along Y=-54km at 1400 with 6km grid length

Fig 7c. Vapour pressure (mb) along Y=-54km at 1400 with 9km grid length

Fig 7d. Vapour pressure (mb) along Y=-54km at 1400 with 12km grid length

Fig 7e. Vapour pressure (mb) along Y=-54km at 1400 with 15km grid length

Fig 8a. Refractivity along Y=-54km at 1500 with 3km grid length

Fig 8b. Refractivity along Y=-54km at 1400 with 6km grid length

Fig 8c. Refractivity along Y=-54km at 1400 with 9km grid length
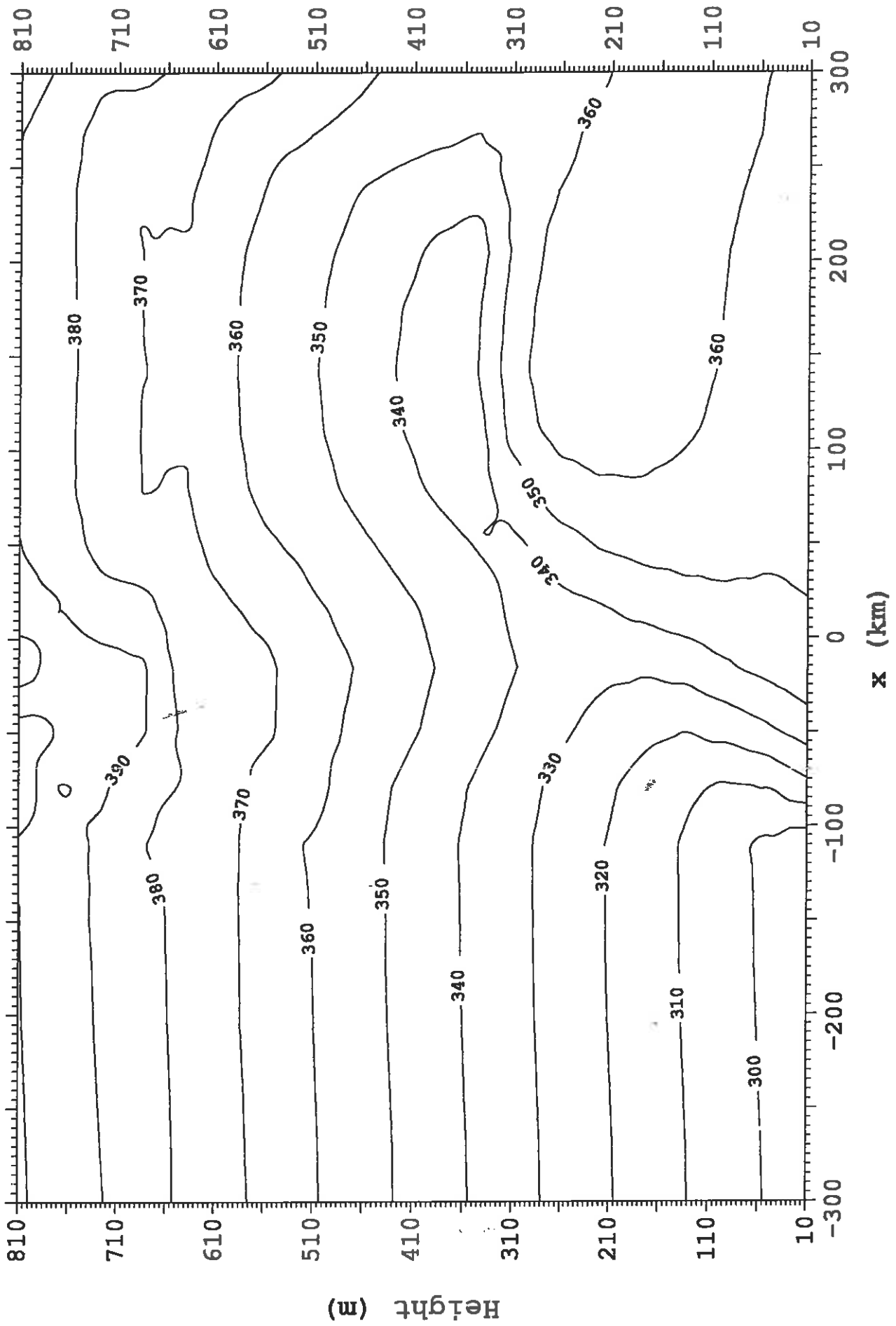
Fig 8d. Refractivity along Y=-54km at 1400 with 12km grid length
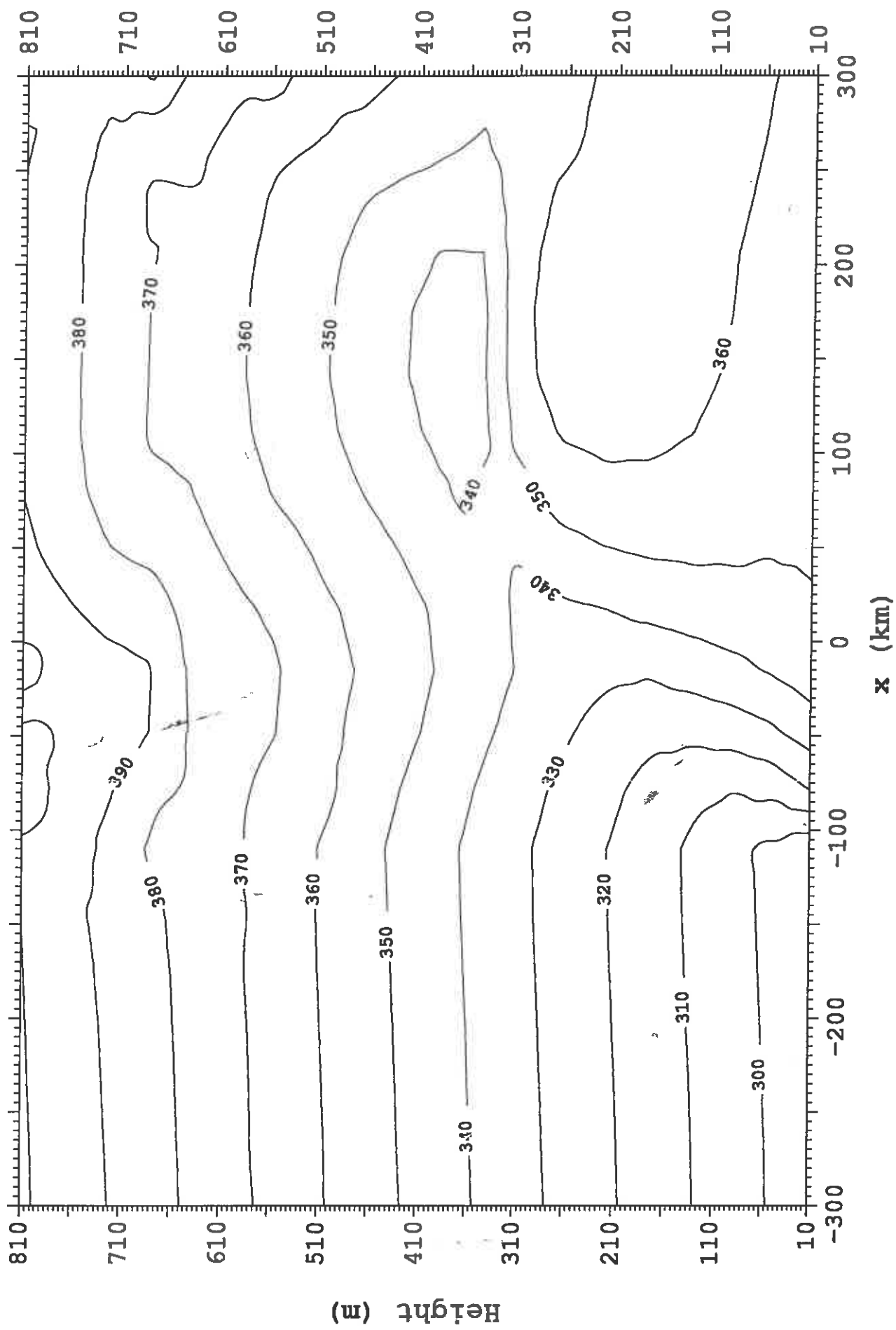
Fig 8e. Refractivity along Y=-54km at 1400 with 15km grid length
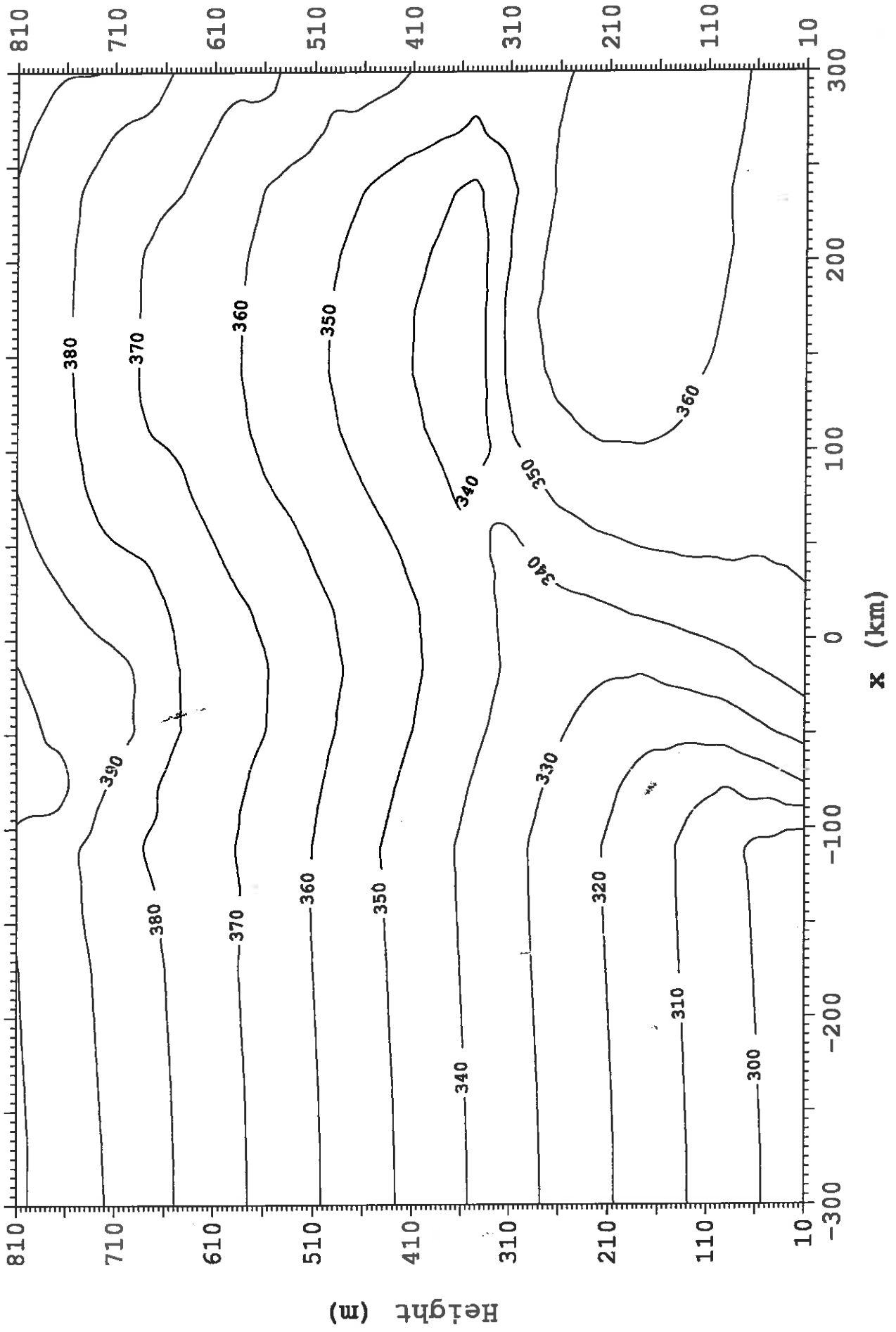
Fig 9a. Winds U (m/s) and W (cm/s) along Y=-54km at 1500 with 3km grid length
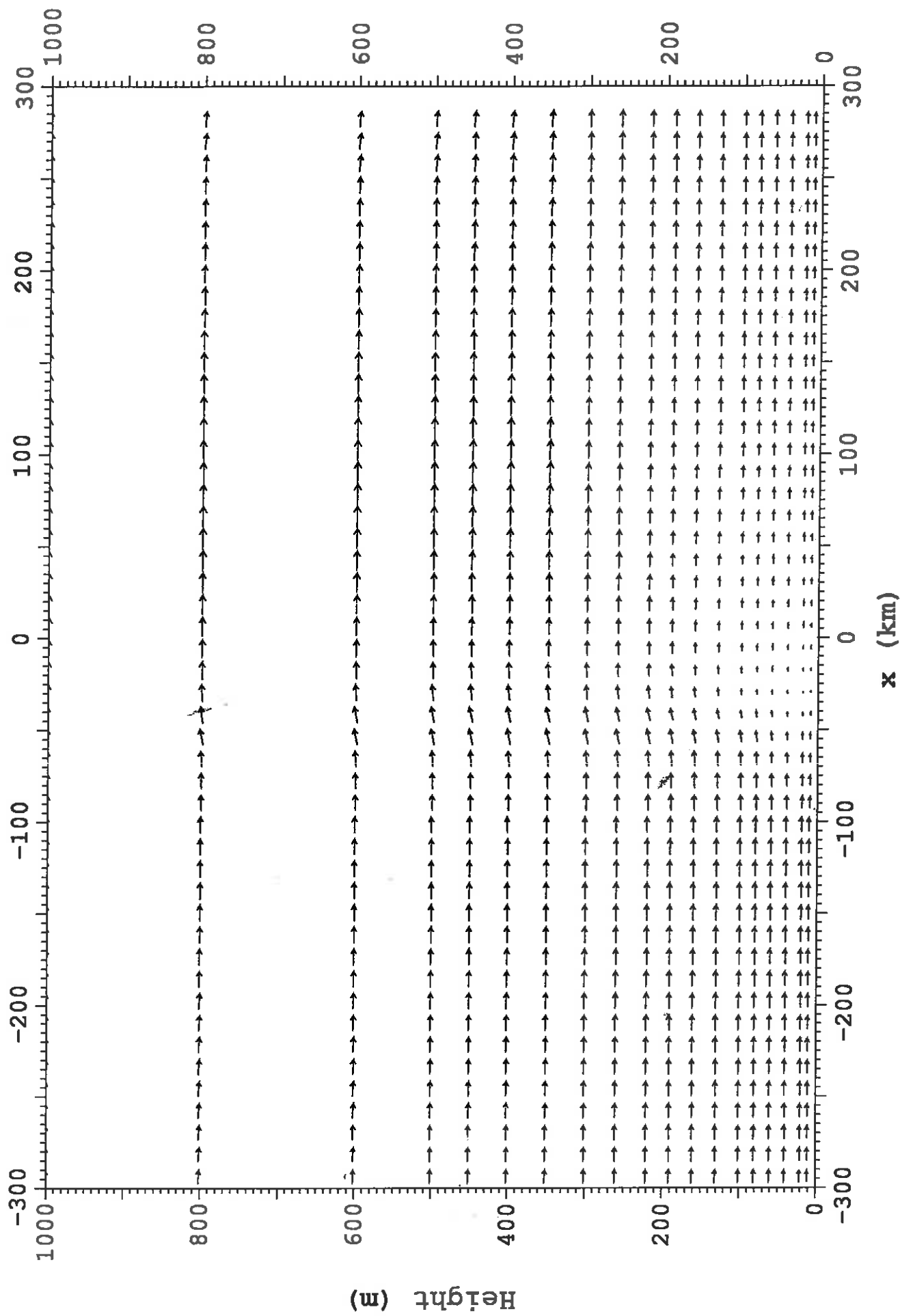
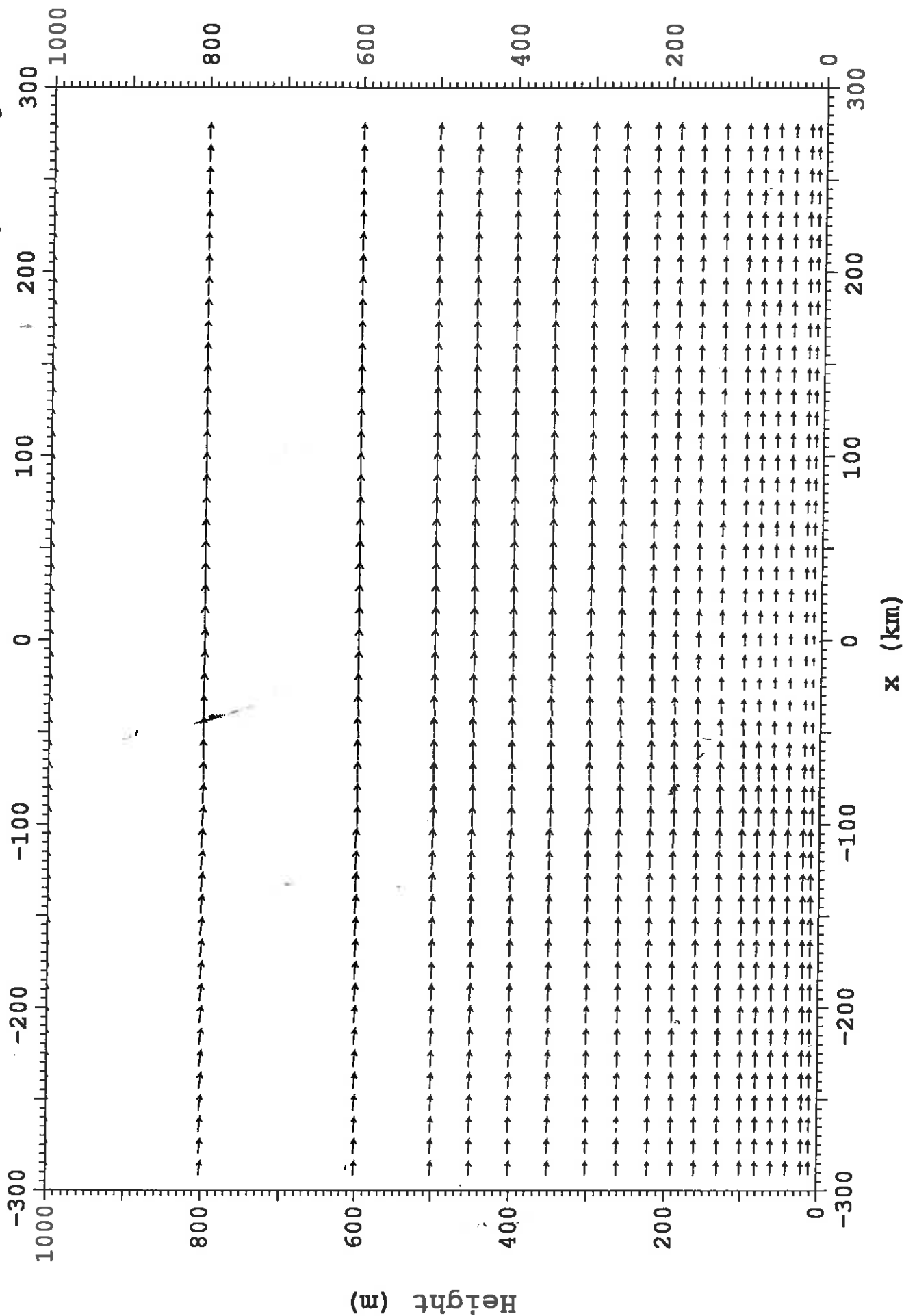Fig 9b. Winds U (m/s) and W (cm/s) along Y=-54km at 1400 with 6km grid length

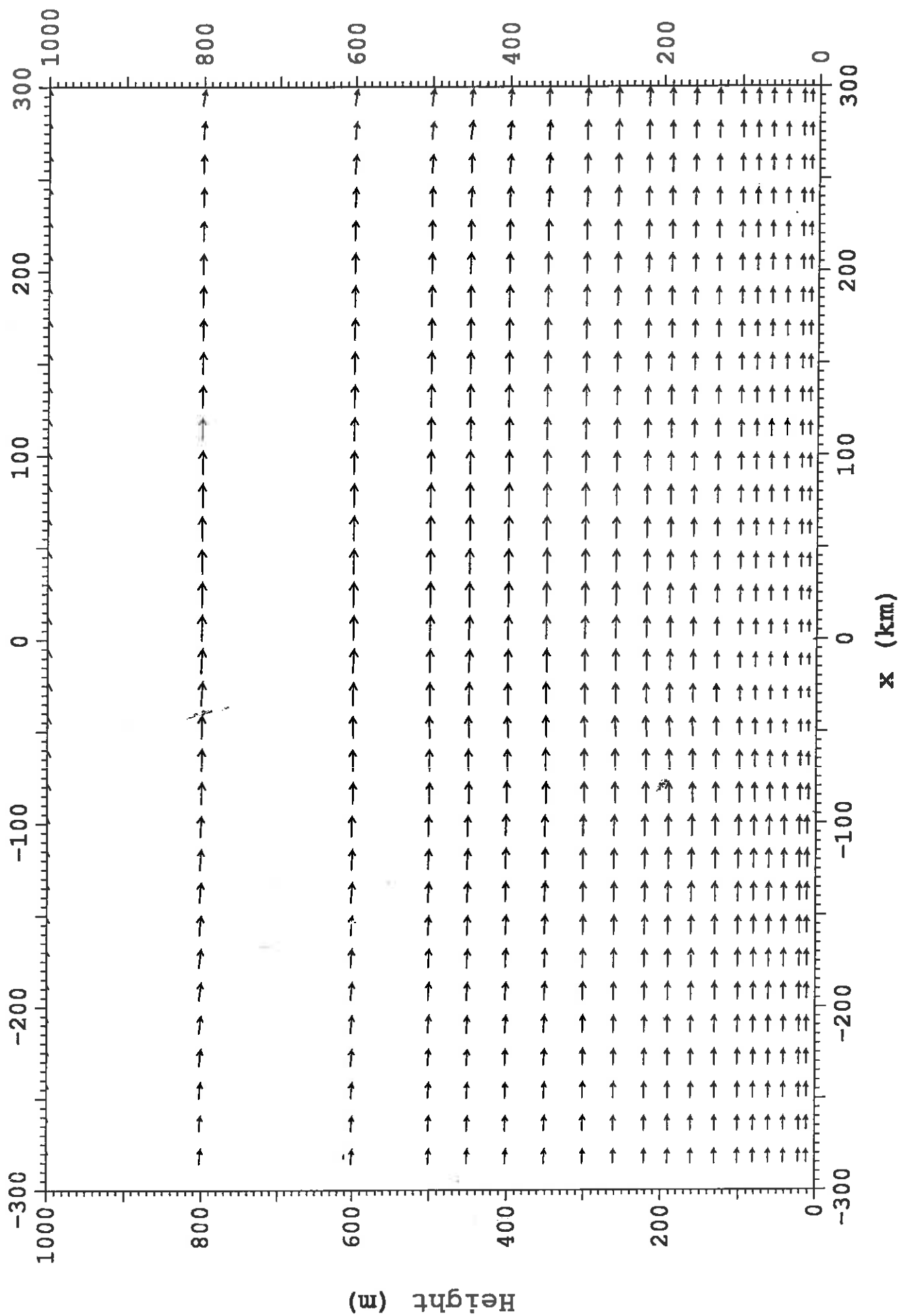Fig 9c. Winds U (m/s) and W (cm/s) along Y=-54km at 1400 with 9km grid length

Fig 9d. Winds U (m/s) and W (cm/s) along Y=-54km at 1400 with 12km grid length
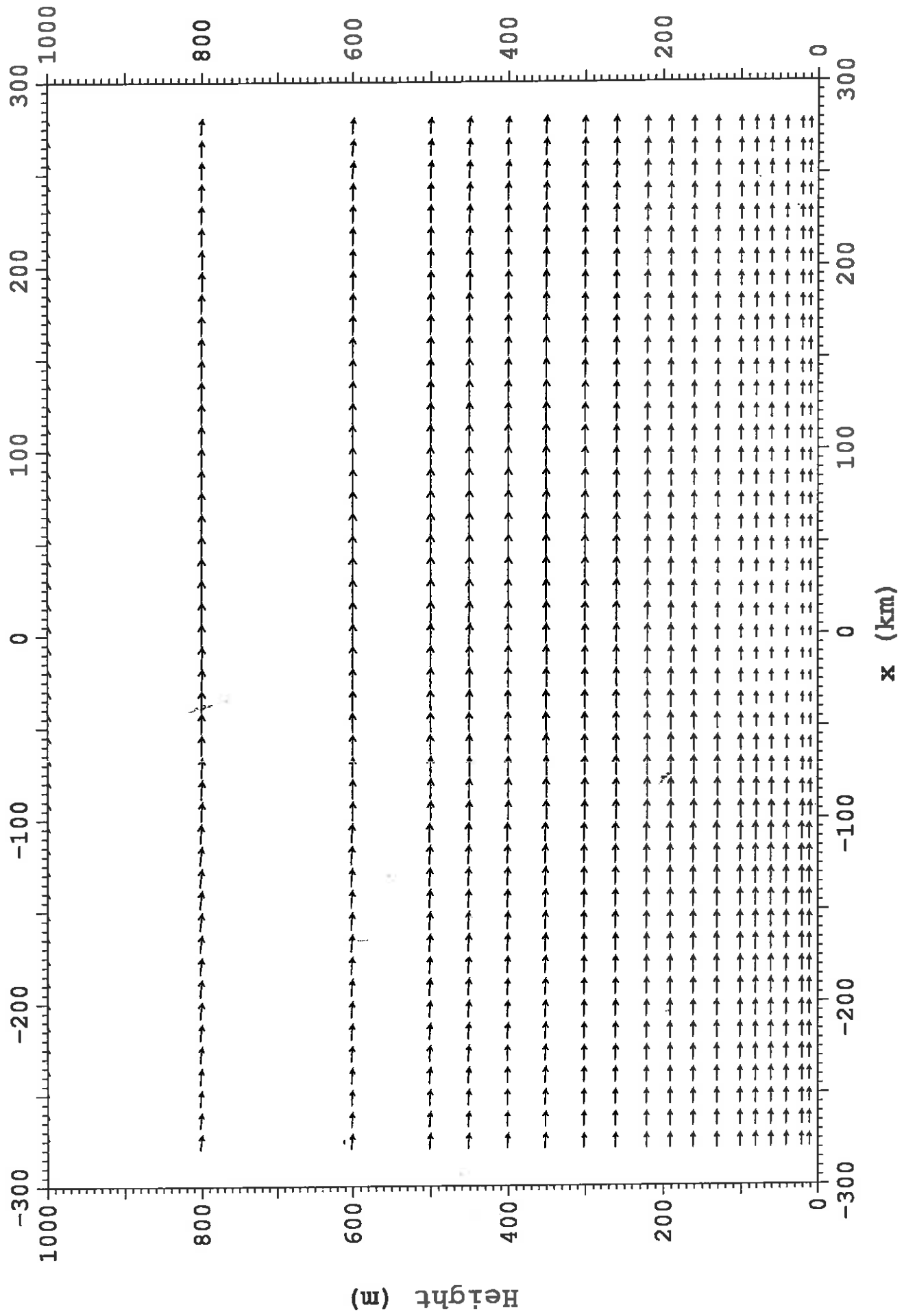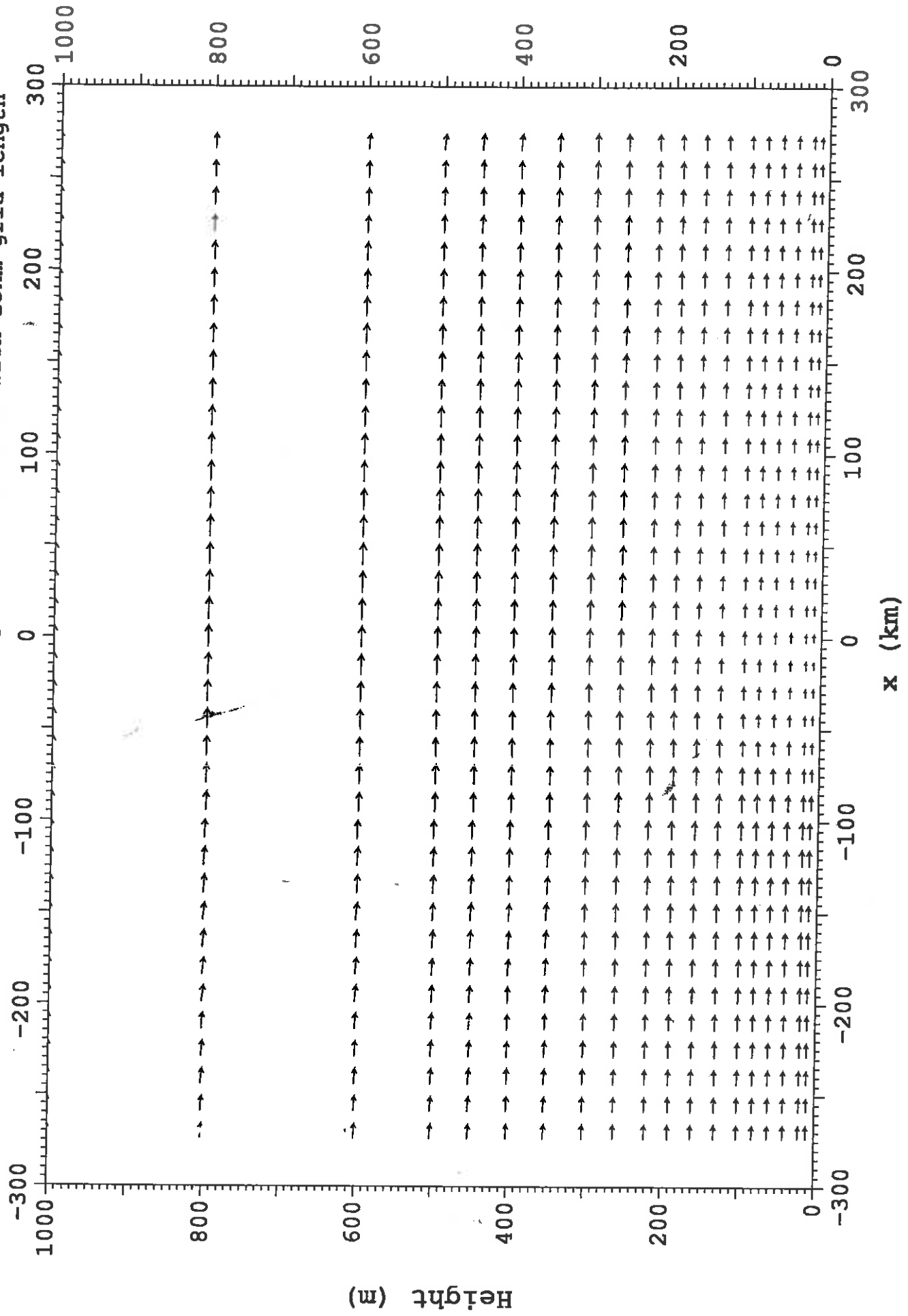

Height (m)

x (km)

Fig 9e. Winds U (m/s) and W (cm/s) along Y=-54km at 1400 with 15km grid length

Fig. 10